


Lack of muscle mTOR kinase activity causes early onset myopathy and compromises whole-body homeostasis

Qing Zhang^{1,2,3,4†‡}, Agnès Duplany^{1,2‡}, Vincent Moncollin^{1,2}, Sandrine Mouradian^{1,2}, Evelyne Goillot^{1,2}, Laetitia Mazelin^{1,2}, Karine Gauthier⁵, Nathalie Streichenberger^{1,6}, Céline Angleraux⁷, Jie Chen⁸, Shuzhe Ding^{3,4}, Laurent Schaeffer^{1,2,6§} & Yann-Gaël Gangloff^{1,2*§} 

¹Institut NeuroMyoGene (INMG), Université Lyon 1, CNRS UMR 5310, INSERM U 1217, Lyon, France, ²LBMC, UMR 5239, ENS Lyon, Lyon Cedex 07, France, ³Key Laboratory of Adolescent Health Assessment and Exercise Intervention of Ministry of Education, East China Normal University, Shanghai, China, ⁴School of Physical Education and Health Care, East China Normal University, Shanghai, China, ⁵Institut de Génomique Fonctionnelle de Lyon, UMR 5242, CNRS, ENS Lyon, Lyon Cedex 07, France, ⁶Centre de Biotechnologie Cellulaire, Hospices Civils de Lyon, Lyon, France, ⁷AniRA PBES, Biosciences Gerland - Lyon Sud (UMS3444/US8), ENS Lyon, Lyon, France, ⁸Department of Cell and Developmental Biology, University of Illinois at Urbana-Champaign, Urbana, IL, USA

Abstract

Background The protein kinase mechanistic target of rapamycin (mTOR) controls cellular growth and metabolism. Although balanced mTOR signalling is required for proper muscle homeostasis, partial mTOR inhibition by rapamycin has beneficial effects on various muscle disorders and age-related pathologies. Besides, more potent mTOR inhibitors targeting mTOR catalytic activity have been developed and are in clinical trials. However, the physiological impact of loss of mTOR catalytic activity in skeletal muscle is currently unknown.

Methods We have generated the mTORMKOKI mouse model in which conditional loss of mTOR is concomitant with expression of kinase inactive mTOR in skeletal muscle. We performed a comparative phenotypic and biochemical analysis of mTORMKOKI mutant animals with muscle-specific mTOR knockout (mTORMKO) littermates.

Results In striking contrast with mTORMKO littermates, mTORMKOKI mice developed an early onset rapidly progressive myopathy causing juvenile lethality. More than 50% mTORMKOKI mice died before 8 weeks of age, and none survived more than 12 weeks, while mTORMKO mice died around 7 months of age. The growth rate of mTORMKOKI mice declined beyond 1 week of age, and the animals showed profound alterations in body composition at 4 weeks of age. At this age, their body weight was 64% that of mTORMKO mice ($P < 0.001$) due to significant reduction in lean and fat mass. The mass of isolated muscles from mTORMKOKI mice was remarkably decreased by 38–56% ($P < 0.001$) as compared with that from mTORMKO mice. Histopathological analysis further revealed exacerbated dystrophic features and metabolic alterations in both slow/oxidative and fast/glycolytic muscles from mTORMKOKI mice. We show that the severity of the mTORMKOKI as compared with the mild mTORMKO phenotype is due to more robust suppression of muscle mTORC1 signalling leading to stronger alterations in protein synthesis, oxidative metabolism, and autophagy. This was accompanied with stronger feedback activation of PKB/Akt and dramatic down-regulation of glycogen phosphorylase expression (0.16-fold in *tibialis anterior* muscle, $P < 0.01$), thus causing features of glycogen storage disease type V.

Conclusions Our study demonstrates a critical role for muscle mTOR catalytic activity in the regulation of whole-body growth and homeostasis. We suggest that skeletal muscle targeting with mTOR catalytic inhibitors may have detrimental effects. The mTORMKOKI mutant mouse provides an animal model for the pathophysiological understanding of muscle mTOR activity inhibition as well as for mechanistic investigation of the influence of skeletal muscle perturbations on whole-body homeostasis.

Keywords mTOR kinase activity; Myopathy; Mitochondria; Glycogen; Body composition

Received: 4 December 2017; Revised: 1 June 2018; Accepted: 25 June 2018

*Correspondence to: Yann-Gaël Gangloff, Institut NeuroMyoGene (INMG), Université Lyon 1, CNRS UMR 5310, INSERM U 1217, Lyon, France. Email: yann-gael.gangloff@univ-lyon1.fr

†Present address: School of Physical Education and Sports Science, Soochow University, Suzhou, China.

‡Q. Zhang and A. Duplany contributed equally to this paper.

§L. Schaeffer and Y.-G. Gangloff contributed equally to this paper.

Introduction

Skeletal muscle integrity is determinant for whole-body health. Alterations of skeletal muscle metabolism and mass have been implicated in the pathogenesis of myopathies, cancer cachexia, and metabolic syndrome as well as in age-related diseases, including sarcopenia. The full understanding of the signalling pathways regulating skeletal muscle homeostasis is thus essential to develop therapeutic strategies aiming to prevent disease and improve quality of life. Body of evidence demonstrates that the mechanistic target of rapamycin (mTOR) signalling pathway is required for muscle growth and metabolism in response to mechanical stimuli, nutrients, growth factors, and hormones.^{1,2} The serine/threonine protein kinase mTOR forms the catalytic core of at least two signalling complexes, the mTOR complex 1 (mTORC1) containing Raptor, which is partially sensitive to rapamycin,³ and the mTORC2 containing Rictor, which is only sensitive to sustained rapamycin treatment.⁴ Pharmacological and genetic approaches have determined that skeletal muscle homeostasis is mainly controlled by mTORC1 signalling. For instance, rapamycin blunts muscle compensatory hypertrophy and recovery after injury, as well as mechanical load-induced growth.^{5–7} Accordingly, mice lacking muscle mTOR (mTORMKO) or Raptor (RAMKO), but not Rictor (RimKO), show reduced muscle mass and develop a late onset myopathy leading to death between the ages of 6 and 8 months.^{8–10} Intriguingly, however, the mass of the slow-twitch/oxidative *soleus* (SOL) muscle is preserved in young mTORMKO mice, while that of the fast-twitch/glycolytic muscles displays a moderate 20–30% reduction, contrasting with the severe inhibitory effect of rapamycin on postnatal muscle growth in rat pups¹¹ and on regenerating myofibre growth.¹² This raises the possibility that the consequences of mTORC1 inactivation in skeletal muscle, using human skeletal actin (HSA)-Cre mice, were previously underestimated due to the supply of mTOR to mutant fibres from unrecombined muscle progenitors during early postnatal muscle growth and muscle regeneration. Indeed, these processes rely on the recruitment of nuclei from satellite cells (SC)^{13–15} in which the HSA-Cre transgene is not active.¹⁶

Paradoxically, sustained activation of muscle mTORC1 in TSC1mKO mice also proved to be detrimental, causing late-onset myopathy,¹⁷ thereby demonstrating that balanced mTORC1 signalling is required for the maintenance of muscle integrity. Indeed, mTORC1 regulates both muscle anabolism and catabolism.¹⁸ The two well-known mTORC1 effectors regulating protein synthesis are the S6 kinases (S6K) and eIF-4E-binding proteins (4E-BP). Noteworthy, S6K KO mice and 4E-BP mutant mice show muscle atrophy but do not develop muscle dystrophy.^{19,20} On the other hand, mTORC1 activity inhibits autophagy-mediated muscle proteolysis through phosphorylation of Unc-51-like kinase-1 (ULK1), transcription factor EB, and PKB/Akt.²¹ Besides protein synthesis

and degradation, mTORC1 controls energy metabolism. mTORC1 promotes the expression of mitochondrial-related genes at the level of transcription and translation, respectively, via the regulation of YY1-PGC-1 α interaction^{22,23} and 4E-BPs.²⁴ Consistently, muscle oxidative capacity is impaired in mTORMKO and RAMKO mice,^{8,9} while enhanced in TSC1mKO mice.²⁵ Although defects in muscle PGC-1 α and YY1 have also been implicated in dystrophic changes,^{23,26} restoring PGC-1 α expression and mitochondrial function in RAMKO and mTORMKO mice does not prevent the myopathy nor extends lifespan.²⁷ Finally, mTORC1 signalling regulates muscle energy stores by controlling glucose metabolism via a feedback inhibition of insulin signalling.²⁸ Accordingly, muscles from mTORMKO and RAMKO mice display enhanced PKB/Akt activation and elevated muscle glycogen stores,^{8,9} whereas muscles with activated mTORC1 show reduced PKB/Akt signalling.¹⁷ Muscle glycogen stores were nevertheless increased in TSC1mKO mice due to enhanced glucose uptake through GLUT1.²⁹

While kinase-independent functions of mTOR have been clearly implicated in myogenesis,³⁰ much less is known in differentiated muscle fibres. To further investigate cell autonomous mTOR catalytic functions in skeletal muscle, we have generated a new mutant mouse model, hereafter called mTORMKOKI (mTOR muscle-specific KnockOut and mTOR Kinase Inactive) mice, in which Cre-mediated mTOR inactivation and expression of an mTOR kinase inactive mutant protein occur conjunctively in differentiated myofibres. This model allowed us to examine the physiological impact of sustained inhibition of mTOR kinase activity in mouse skeletal muscle. Our comparative analysis reveals exacerbated alterations in mTORMKOKI mice compared with mTORMKO littermates. It further indicates that catalytic-independent functions of mTOR do not rescue any parameters found to be altered in mTOR-depleted muscle fibres and, unexpectedly, that muscle mTOR determines the mass of peripheral organs. Collectively, our results demonstrate that the importance of muscle mTOR was underestimated in previous mouse models of mTORC1 inactivation.

Methods

Animals

The generation of animals harbouring conditional *mTOR* alleles (*mTOR*^{fl α /fl α}) and of animals with muscle-specific mTOR inactivation (*HSA-Cre*⁺; *mTOR*^{fl α /fl α} herein called mTORMKO) on F6; C57BL/6 background has been previously described in Risson *et al.*⁹ Transgenic mouse lines overexpressing FLAG-tagged Kinase Inactive (Asp2357Glu) human mTOR (herein called mTORMKI) or FLAG-tagged human mTOR (herein called mTORMWT) in skeletal muscle have been previously

described in Ge *et al.*¹² For this study, mTORMKI and mTORMWT mouse lines were outcrossed six times to C57BL/6 background. They were next bred with *mTOR^{flox/flox}* mice to generate mice homozygous for the mTORflox locus. On the one hand, mTORMKI mice were then bred with mTORMKO mice to generate the following littermates: Control, mTORMKI, mTORMKO, and mTORMKOKI, the latest being knockout for the muscle mTORflox locus while overexpressing an mTOR kinase inactive protein from the transgene. On the other hand, mTORMWT mice were then bred with mTORMKO mice to generate the following littermates: Control, mTORMWT, mTORMKO, and mTORMKOWT, the latest being knockout for the muscle mTORflox locus while overexpressing mTOR from the transgene.

The animals were provided with mouse chow and water ad libitum under a light–dark cycle (12 h), in a restricted-access, specific pathogen–free animal care facility at AniRA PBES, Lyon, France. For experimental convenience, the animals analysed were males, unless otherwise stated. Experiments were conducted using littermates from multiple litters. To minimize physiological variation, mTORMKOKI male mice that did not reach 7 g at 4 weeks of age were excluded from analysis. All procedures were performed in accordance with French and European legislation on animal experimentation and approved by the ethics committee CECCAPP and the French ministry of research.

PCR genotyping was performed with the following primers:
 mTORflox Fw: GCTCTTGAGGCAAATGCCACTATCACCC
 mTORflox Rev: TCATTACCTTCTCATCAGCCAGCAGTT
 mTORKI/mTORWT Fw: CCTCGTCTCCGAGCCACAC
 mTORKI/mTORWT Rev: ACTCATCTCTCGGAGTTCCATGG
 Cre Fw: CGATGCAACGAGTGATGAGG
 Cre Rev: GCATTGCTGTCACTTGCTCGT

Muscle histology, morphometric measurements, and imaging

Tibialis anterior (TA) and SOL muscles were collected, embedded in tragacanth gum, and quickly frozen in isopentane cooled in liquid nitrogen. Cross-sections (10 µm thick) were obtained from the middle portion of frozen muscles and processed for histological, immunohistochemical, enzymohistological analysis according to standard protocols. The fibre cross-sectional area and the number of centrally nucleated fibres were determined on TRITC-labelled WGA (L5266, Sigma) and DAPI-stained sections. Number of peripheral myonuclei were determined on WGA-Alexa 488 (W1161, Invitrogen TM) and DAPI-stained sections. Fluorescence microscopy and transmission microscopy were performed using Axioimager Z1 microscope with CP Achromat 5x/0.12, 10x/0.3 Ph1, or 20x/0.5 Plan NeoFluar objectives (Carl Zeiss, Inc.). Images were captured using a charge-coupled device monochrome camera (Coolsnap HQ;

Photometrics) or colour camera (Coolsnap colour) and MetaMorph software. For all imaging, exposure settings were identical between compared samples. Fibre number and size, central nuclei and peripheral myonuclei were calculated using ImageJ software.

Quantitative real-time PCR

Total RNA was prepared from frozen TA, SOL, or *extensor digitorum longus* muscles using TRIzol (TRI-Reagent, Sigma). Complementary DNA was generated using RevertAid H minus Reverse transcriptase (Fermentas) and random hexamer primers. Real-time quantitative PCR was carried out using QuantiFast SYBR Green (Qiagen). All data were normalized to cyclophilin B and GAPDH mRNA levels, which gave similar results. Delta Delta Ct (threshold cycle) analysis was used to calculate relative gene expression. The results were plotted in arbitrary units as mean ± SEM. The sequences of the forward and reverse primers were as follows: mouse mTOR, 5'-CAAACCACAGGGTGAGGACT-3' and 5'-AGGGCAGCAACAGT GAGAGT-3'; mouse Myh8, 5'-CAAGGATGGAGGGAAAGTGA-3' and 5'-GGTTCATGGGGAAGACTTGA-3'; mouse Myogenin, 5'-CTACAGGCCTTGCTCAGCTC-3' and 5'-AGATTGTGGCGTCTG TAGG-3'; mouse IGF-II, 5'-ACCCGACCTTCGGCCTTG-3' and 5'-AAGCCGCGGTCCGAACAGAC-3'; mouse PGC-1α, 5'-TCAC ACCAAACCACAGAAA-3' and 5'-TCTGGGGTCAGAGGAA GAGA-3'; mouse Dystrophin, 5'-TGCGTATCAGGAGACAATG-3' and 5'-TTCTTGCCATCTCCTTAC-3'; mouse Cyclophilin B, 5'-GATGGCACAGGAGGAAAGAG-3' and 5'-AACTTGGCCGAAAA CCACAT-3'; mouse GAPDH, 5'-GGTACCAGGGCTGCCATTG-3' and 5'-TTCCAGAGGGCCATCCACAG-3'; mouse PPARα, 5'-GCGTACGGCAATGGCTTTAT-3' and 5'-ACAGAACGGCTTCTCCT AGGTT-3'; mouse PPARδ, 5'-CTCTTCATCGCGGCCATCATTCT-3' and 5'-TCTGCCATCTTCTGCAGCAGCTT-3'; mouse MCAD, 5'-ACTGACGCCGTTTTCAGATTTT-3' and 5'-GCTTAGTTACACGA GGGTGATG-3'; mouse LCAD, 5'-ATGGCAAATACTGGGCATC-3' and 5'-TCTTGCATCAGCTCTTCA-3'; mouse CPT2, 5'-CCAGCTGACCAAAGAAGCA-3' and 5'-GCAGCCTATCCAGTCA TCGT-3'; mouse FABP3, 5'-GACGAGGTGACAGCAGATGA-3' and 5'-TGCCATGAGTGAGAGTCAGG-3'; mouse HADH, 5'-AACTGCGTTCATCAAACC-3' and 5'-TCCCTCAAATATGCCT TTGG-3'; mouse FGF21, 5'-TACACAGATGACGACCAAGA-3' and 5'-GGCTTCAGACTGGTACACAT-3'.

Immunoblotting

Gastrocnemius (GC), TA, and SOL muscles from at least three mice per genotype were dissected and snap-frozen in liquid nitrogen until use. Tissues were crushed with beads in a homogenizer system (FastPrep-24, MP Biomedicals) in 20 mM tris-HCl (pH 8.0), 138 mM NaCl, 5% glycerol, 1% Nonidet P40, 5 mM EDTA, 1 mM Dithiothreitol with protease and

phosphatase inhibitors from Roche. Lysates were then centrifuged at 20 000 *g* for 15 min. Protein concentration was calculated using the Biorad's DC Protein Assay. Equal amounts of proteins were subjected to western blot analysis. Antibodies used: 4EBP1 (#9452; Cell Signaling), phospho-4EBP1 (T37/46; #2855; Cell Signaling), Akt (#9272; Cell Signaling), phospho-Akt (S473; #9271; Cell Signaling), phospho-Akt1 (S473; #9018; Cell Signaling), phospho-Akt2 (S474; #8599; Cell Signaling), phospho-Akt (S308; #4056; Cell Signaling), AS160 (#2670; Cell Signaling), phospho-AS160 (S588; #8730; Cell Signaling), phospho-ULK1 (S757; #6888; Cell Signaling), phospho-ULK1 (S317; #6887; Cell Signaling), anti-mTOR (#2983; Cell Signaling), phospho-mTOR (S2448; #2971; Cell Signaling), IRS1 (#2382; Cell Signaling), GAPDH (#4978; Cell Signaling), S6 (#2217; Cell Signaling), phospho-S6 (S240/244; #2215; Cell Signaling), α -Tubulin (T6074; Sigma), GPh (sc66913; Santa Cruz Biotechnology), myoglobin (sc8080; Santa Cruz Biotechnology), Complex IV subunit I (MS404-SP; Mitosciences), FGF21 (Ab171941; Abcam).

Transmission electron microscopy

Tibialis anterior muscle was dissected and immediately fixed with 2% glutaraldehyde and postfixed with 2% osmium tetroxide in 0.3 M sodium cacodylate buffer pH 7.4. TA muscle was then dehydrated and embedded in Epon epoxy resin. Ultra-thin sections (70 nm) were cut with ultramicrotome Leica Ultracut UCT and contrasted with uranyl acetate. Sections were examined with a JEM-1400 TEM (Jeol) operated at an accelerating voltage of 80 KV and equipped with an Orius CCD Camera (Gatan). Digital images were recorded and processed with the Digital Micrograph Software (Gatan).

Metabolic measurements

Blood glucose levels were determined from tail venous blood using an automatic glucose monitor (Roche). Serum levels of insulin were determined with rat/murine ELISA kit (MERCK). For glucose tolerance tests, 4-week-old mice were fasted 5 h and injected intraperitoneally with 2 mg glucose/g body weight. For insulin resistance tests, 5 h fasted mice were injected intraperitoneally with insulin (0.75 mUI/g body wt; Sigma-Aldrich).

Glycogen quantification

Glycogen was obtained by 28% KOH treatment of the TA or GC muscle, heating at 100°C for 2 h followed by precipitation with EtOH at -80°C and centrifugation at 18 000 *g* at 4°C. The resulting pellet was resuspended in development buffer, and muscle glycogen amount was assessed using glycogen

Assay kit II colorimetric (Abcam #ab169558). The absorbance spectrum was recorded at 450 nm.

Polysome analysis

Sucrose density gradient centrifugation was used to separate the subpolysomal from the polysomal fractions as described in Mazelin *et al.*³¹ For each profile, a pool of 3 to 5 frozen GC muscle (100 mg) was homogenized with ultraturax in 50 mM tris-HCl (pH 7.4), 10 mM MgCl₂, 250 mM KCl, 7 mM β -mercaptoethanol, 0.18 mM Cycloheximide. To remove cell debris, homogenates were spun at 4000 \times *g* for 10 min at 4°C. Pellets were resuspended in buffer containing 1% Triton X-100, 0.5% sodium deoxycholate and spun at 4000 \times *g* for 10 min at 4°C. Supernatant from both centrifugations were pooled and spun at 20 000 \times *g* for 20 min at 4°C to obtain cytosolic supernatant. An aliquot of the supernatant was used to measure protein concentration. Same protein amount were layered on a 10–50% linear sucrose gradient (50 mM tris-HCl (pH 7.4), 10 mM MgCl₂, 250 mM KCl, 7 mM β -mercaptoethanol, 0.18 mM Cycloheximide) and centrifuged in a SW41 rotor at 200 000 *g* for 2 h at 4°C. One millilitre fractions were collected using a Piston Gradient Fractionator coupled to the BioLogic LP chromatography system (Bio-Rad) with continuous measurement of the absorbance at 254 nm. Polysome profiles were performed twice per genotype and per age.

Statistical analysis

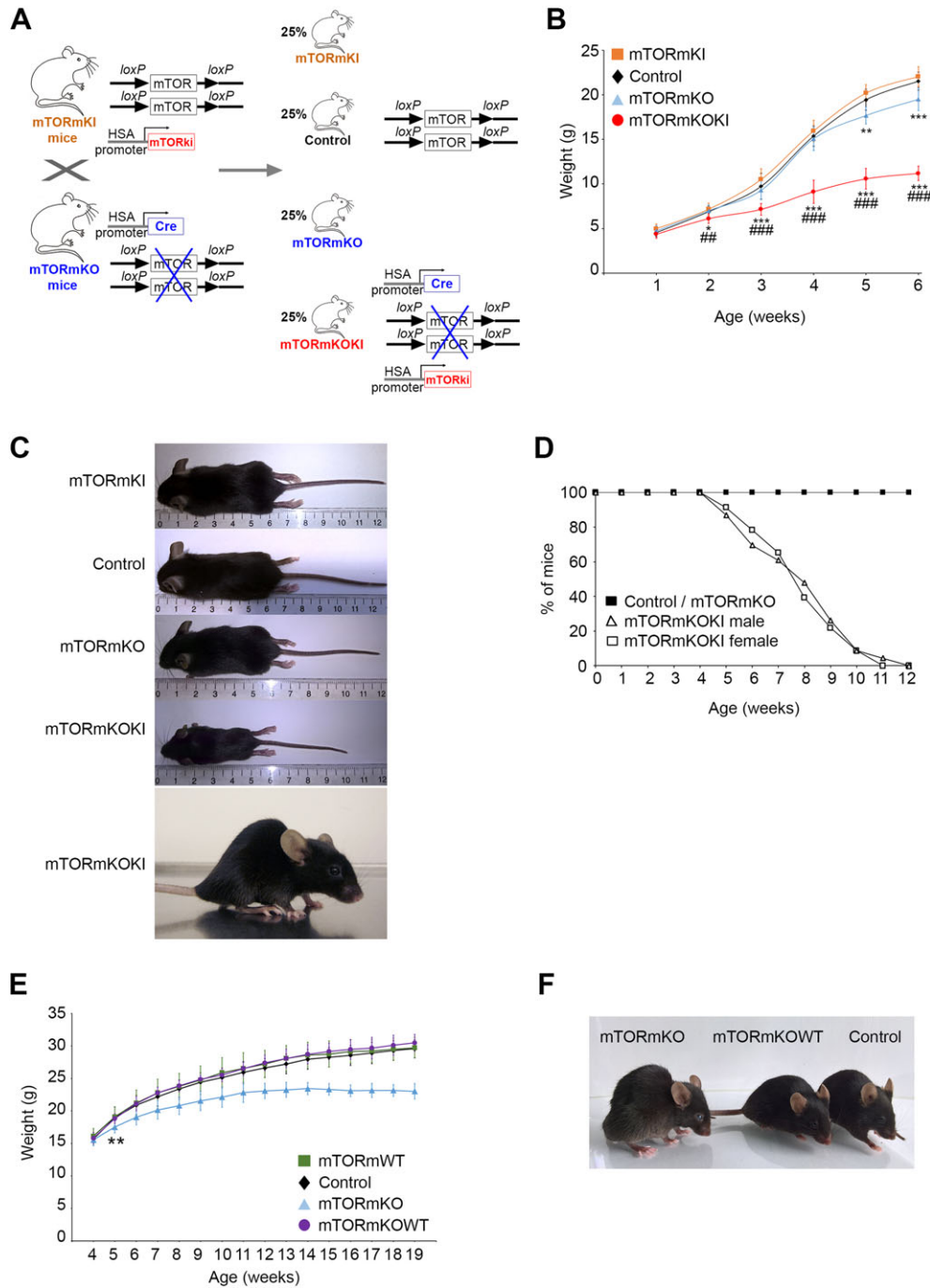
Statistical comparison of the three groups was performed using the nonparametric Wilcoxon sign-rank test with R©, version 3.4.1. Results are expressed as mean \pm SEM or SD, and $P < 0.05$ was considered significant.

Results

mTORMKOKI mice exhibit postnatal growth failure and short lifespan

To address the cell autonomous significance of mTOR catalytic activity in skeletal muscle homeostasis, we have generated the mTORMKOKI mouse line that is defective in endogenous muscle mTOR while expressing an mTOR kinase inactive (mTORki) protein. This mutant line was obtained by crossing muscle-specific mTOR knockout mice expressing Cre recombinase in skeletal muscle and carrying mTOR floxed alleles (hereafter called mTORMKO)⁹ with transgenic mice expressing a FLAG-tagged kinase-inactive (Asp2357Glu) human mTOR protein in skeletal muscle¹² and carrying mTOR floxed alleles (hereafter called mTORMKI mice) (Figure 1A and

Figure 1 Characterization of mTOR mutant mice. (A) Strategy to generate the mTOR mutant mouse models. (B) Growth curve of mTORmKI ($n = 11$), mTORmKO ($n = 11$), mTORmKOKI ($n = 10$), and Control ($n = 11$) male mice ($n \geq 10$ per genotype) between week 1 and 6. (C) Morphology of mTORmKI, Control, mTORmKO, and mTORmKOKI mice at 4 weeks of age. (D) Survival curve of mTOR mutant and control mice ($n = 23$). (E) Growth curve of mTORmWT ($n = 11$), mTORmKO ($n = 11$), mTORmKOWT ($n = 10$), and Control ($n = 11$) male mice between week 4 and 19. (F) Morphology of mTORmKO, mTORmKOWT, and Control mice at 23 weeks of age. Data indicate mean \pm SD. $^*/\#P < 0.05$; $^{**}/\#\#P < 0.01$; $^{***}/\#\#\#P < 0.001$, * is mTOR mutant vs. Control, # is mTORmKOKI vs. mTORmKO.



Supporting Information, Table S1). As expression of both Cre and mTOR^{ki} relies on the HSA promoter, Cre-mediated recombination of the endogenous mTOR^{lox} locus in mTOR^{mKOKI} muscles is conjunctively associated with expression of mTOR^{ki}. Consideration should be given to the activity of the HSA promoter that is restricted to fused myotubes and differentiated myofibres throughout embryonic and postnatal development but is lacking in myoblasts and SC.^{16,32} The four genotypes among the offsprings of these crosses, including mTOR^{lox/lox} (control mice), mTOR^{lox/lox} HSA-KI-mTOR (mTOR^{mKI} mice), mTOR^{lox/lox} HSA-Cre⁺ (mTOR^{mKO} mice) and mTOR^{lox/lox} HSA-KI-mTOR (mTOR^{mKOKI} mice), were obtained in mendelian ratio and phenotypically indistinguishable at birth. As expected from previous studies,¹² mTOR^{mKI} mice did not display obvious phenotype (Figure 1B and 1C). Indeed, an mTOR^{ki}/mTOR^{wt} ratio of 2 to 3 in skeletal muscle was shown to be insufficient to lead to dominant-negative effects.¹² Consistently with our previous observations,⁹ mTOR^{mKO} littermates displayed little but significant reduced body weight starting from 5 weeks of age as well as late onset myopathy as spinal deformation appeared at ~13 weeks of age and the animals died around 7 months of age. Surprisingly, the growth rate of mTOR^{mKOKI} mice declined beyond 1 week of age and the animals showed a rapid progression of leanness, kyphosis, and weakness (Figure 1B and 1C). More than 50% mTOR^{mKOKI} mice died before 8 weeks of age and none survived more than 12 weeks (Figure 1D). Near death, mTOR^{mKOKI} mice became prostrated and subsequently succumbed most likely from the inability to eat contrasting with the primary cause of death of mTOR^{mKO} mice attributed to respiratory failure.⁹

To exclude a contribution of the FLAG epitope and/or of the human-derived mTOR protein in the exacerbated mTOR^{mKOKI} phenotype, we generated the mTOR^{mKOWT} (mTOR^{muscle-specific KnockOut} and mTOR^{Wild Type}) mouse line by crossing mTOR^{mKO} mice with a transgenic mouse line expressing a FLAG-tagged human mTOR in skeletal muscle¹² and carrying mTOR floxed alleles (hereafter called mTOR^{mWT} mice) (Supporting Information, Table S1). The mTOR^{mKOWT} mice obtained from these crosses were indistinguishable from Control and mTOR^{mWT} littermates all throughout their life (Figure 1E and 1F). Thus, the FLAG-tagged human mTOR protein rescued the pathophysiology of mTOR^{mKO} mice, demonstrating its ability to compensate for muscle mouse mTOR.

Given the small size of the mTOR^{mKOKI} mice, we investigated the weight of various organs and tissues before weaning at 4 weeks of age. At this age, mTOR^{mKO} and control mice had similar body weights while it was reduced by 37% in mTOR^{mKOKI} mice (Table 1). Importantly, the weights of skeletal muscles and major organs examined were remarkably lighter in mTOR^{mKOKI} mice as compared with Control and mTOR^{mKO} mice, while only the weights of TA and GC muscles in mTOR^{mKO} mice were reduced as compared with Controls. In contrast, no differences between the groups

Table 1 mTOR^{mKOKI} mice display a strong reduction in skeletal muscle and peripheral organ weights with compared to mTOR^{mKO} mice

Variable	Control	mTOR ^{mKO}	% of control	mTOR ^{mKOKI}	% of control	% of mTOR ^{mKO}
Body weight (g)	15.83 ± 0.55	15.64 ± 1.12	99	10.02 ± 1.39 ***/###	63	64
TA weight (mg)	23.53 ± 1.34	19.33 ± 1.77 ***	82	11.79 ± 1.77 ***/###	50	61
TA / BW (mg/g)	1.49 ± 0.11	1.24 ± 0.05 ***	83	1.18 ± 0.14 **	79	96
SOL weight (mg)	4.08 ± 0.36	3.96 ± 0.53	97	1.74 ± 0.51 ***/###	43	44
SOL / BW (mg/g)	0.26 ± 0.02	0.26 ± 0.04	99	0.17 ± 0.05 **/###	68	68
GC weight (mg)	50.99 ± 4.25	42.17 ± 3.85 ***	83	25.99 ± 3.97 ***/###	51	62
GC / BW (mg/g)	3.23 ± 0.27	2.70 ± 0.12 **	84	2.60 ± 0.20 ***	81	96
Liver (mg)	959.25 ± 134.99	942.04 ± 97.92	98	581.90 ± 90.44 ***/###	61	62
Liver / BW (mg/g)	60.60 ± 8.34	60.25 ± 4.66	99	58.24 ± 5.20	96	97
Heart weight (mg)	96.96 ± 10.86	91.60 ± 8.03	94	69.45 ± 6.31 ***/###	72	76
Heart / BW (mg/g)	6.13 ± 0.72	5.86 ± 0.40	96	6.84 ± 0.96 **/###	112	117
Kidney (mg)	107.24 ± 6.55	110.02 ± 11.82	103	83.42 ± 10.86 ***/###	78	76
Kidney / BW (mg/g)	6.78 ± 0.36	7.04 ± 0.53	104	8.35 ± 0.48 ***/###	123	119
Gonadal fat pads weight (mg)	85.29 ± 14.58	82.99 ± 14.62	97	32.87 ± 15.86 ***/###	39	40
Gonadal fat pads / BW (mg/g)	5.38 ± 0.83	5.32 ± 0.94	99	3.18 ± 1.36 **/###	59	60
Tibia (mm)	138.75 ± 7.64	139.67 ± 6.94	101	137.88 ± 4.72	99	99
Femur (mm)	108.13 ± 8.54	107.00 ± 8.19	99	104.76 ± 6.42	97	98

Values are for 4-w control (n=8), mTOR^{mKO} (n=10) and mTOR^{mKOKI} (n=12) male mice. The data are means ± SD.

*#P < 0.05.

**/###P < 0.01.

***/###P < 0.001, * is mTOR mutant vs. Control, # is mTOR mutant vs. mTOR^{mKO}. Abbreviations: TA, Tibialis Anterior; SOL, Soleus; GC, Gastrocnemius.

were found in the lengths of the tibias and femurs. Normalization to body weight showed that all skeletal muscles examined and white adipose tissues were disproportionately reduced in mTORmKOKI mice, but only TA and GC muscles were similarly affected in mTORmKO mice (Table 1). Therefore, mTORmKOKI mice were smaller than mTORmKO littermates due to a general decrease in organ size, skeletal muscle, and white adipose tissues being more severely affected. Collectively, these results reveal that muscle mTOR kinase is crucial for mouse postnatal muscle growth and, unexpectedly, also for whole-body homeostasis.

Dystrophic features are exacerbated in mTORmKOKI as compared with mTORmKO mice

We next examined the histology of the slow-twitch oxidative SOL and fast-twitch glycolytic TA muscles in mTOR mutant mice at 6 weeks of age. At this age, mTORmKO and mTORmKOKI mice were respectively 93% and 59% the weight of Control littermates (Figure 2A). The weights of SOL and TA muscles from mTORmKOKI mice were respectively 42% and 50% those of Controls, while in mTORmKO mice, they were respectively not significantly different to and 80% those of Controls. Muscle fibre size was next determined in SOL and TA muscles from Controls and mTOR mutant mice (Figure 2B). Mean fibre size was similar in Control and mTORmKO SOL muscles ($1396 \pm 66 \mu\text{m}^2$ vs. $1357 \pm 29 \mu\text{m}^2$) consistently with our previous findings,⁹ whereas it was severely reduced in mTORmKOKI SOL fibres ($808 \pm 24 \mu\text{m}^2$). In mTORmKOKI TA muscle, mean fibre size was significantly smaller ($1296 \pm 13 \mu\text{m}^2$) than in mTORmKO TA ($1625 \pm 34 \mu\text{m}^2$) and Control TA muscle ($2066 \pm 35 \mu\text{m}^2$). Accordingly, both mTORmKOKI TA and SOL muscles displayed a downshift of myofibre size distribution relative to mTORmKO muscles (Supporting Information, Figure S1A and S1B). Noteworthy, the total number of muscle fibres did not significantly change between the three genotypes (data not shown), indicating that mTORmKOKI muscles were lighter than mTORmKO muscles due to reduced fibre size. Early postnatal muscle fibre hypertrophy in mice is achieved by accretion of myonuclei provided by SC, whose number is established 3 weeks after birth.¹³ We therefore investigated the number of peripheral myonuclei in mTORmKOKI muscle fibres. However, TA muscle fibres from all three genotypes contained comparable amount of peripheral myonuclei (Supporting Information, Figure S2A) indicating that the mTORmKOKI phenotype is not due to a deficit in postnatal SC nuclei accretion. At 6 weeks of age, both mTOR mutant lines displayed dystrophic alterations prominently in SOL muscle (Figure 2C and Supporting Information, Figure S2B). However, they were exacerbated in mTORmKOKI as compared with mTORmKO mice and dominated by small fibres with recurrent nuclear centralization indicative of regenerating fibres.

In agreement with these observations, the percentage of fibres with centrally located nuclei was much higher in mTORmKOKI than mTORmKO muscles (Figure 2D). Further evidence of higher regeneration rates in mTORmKOKI mice was demonstrated at the molecular level by the greater induction of perinatal muscle myosin heavy chain MyH8, IGF2, and myogenin in the slow-twitch SOL muscle (Figure 2E) as well as in the fast-twitch TA (Supporting Information, Figure S2C) and *extensor digitorum longus* (Supporting Information, Figure S2D) muscles. These observations confirm previous findings showing that mTOR kinase activity is dispensable for nascent myofibre formation during regeneration.¹² In addition, hematoxylin eosin saffron staining showed a significant increase in inter-fibre spacing and fibrosis in mTORmKOKI SOL muscle (Figure 2C). Gomori trichrome and Sudan black staining revealed excessive accumulation of mitochondria (red dots) and lipid droplets (blue dots) in mTORmKOKI as compared with mTORmKO SOL muscle fibres, indicative of a mitochondrial disorder. Finally, SOL muscle from mTORmKOKI but not from mTORmKO mice displayed adipose infiltration (Supporting Information, Figure S2E). Therefore, muscle pathological changes were early and more severe in mTORmKOKI as compared with mTORmKO mice. These data further reveal that inhibition of muscle mTOR catalytic activity is highly detrimental to muscle integrity.

Muscle mTOR kinase activity is essential for the regulation of dystrophin as well as for PPARs/PGC-1 α -mediated mitochondrial oxidative capacity and lipid utilization in vivo

Down-regulation of dystrophin and peroxisome proliferator-activated receptor- γ coactivator α (PGC-1 α) transcripts in muscles from mTORmKO mice has been shown to contribute to the pathogenesis of their myopathy.⁹ While initial studies support mTOR catalytic-independent and -dependent mechanisms as means by which mTOR respectively controls dystrophin and PGC-1 α transcription,^{9,23} mTOR activation in TSCmKO mice was also shown to decrease muscle PGC-1 α transcripts.²⁵ The mTORki mutation in mTORmKOKI mice allowed us to determine whether muscle mTOR catalytic activity was directly involved in the regulation of the expression of these genes. Both dystrophin and PGC-1 α mRNA transcripts were strongly down-regulated in SOL muscle from mTORmKOKI mice at 4 and 6 weeks of age (Figure 3A and 3B). Similarly, expression of myoglobin, a PGC-1 α target gene, as well as that of the mitochondrial-encoded cytochrome c oxidase subunit 1 (complex IV) was markedly decreased at both ages (Figure 3C and Supporting Information, Table S2). These results contrasted with the mild changes observed in SOL muscle from 4-week-old (4-w) mTORmKO mice. Conversely, the deficit in expression of these markers was clear in SOL muscle from 6-w mTORmKO mice (Figure 3A–C and

Figure 2 mTORmKOKI mice exhibit exacerbated dystrophic features. (A) Body weight as well as SOL and TA mass from 6-w mTORmKO ($n = 7$) and mTORmKOKI ($n = 8$) mice relative to Controls ($n = 7$). (B) SOL and TA muscle mean fibre cross-sectional area (CSA) in 6-w Control, mTORmKO, and mTORmKOKI male mice. Fibre CSA was determined on TRITC-labelled WGA-stained sections as described in the methods section. This analysis includes a minimum of 400 myofibres per SOL muscle and 1200 myofibres per TA muscle from three mice per genotype. (C) Representative Hematoxylin & Eosin (upper panel), Gomori trichrome (middle panel), and Sudan black (lower panel) staining of *soleus* muscle sections from 6-w Control, mTORmKO, and mTORmKOKI mice. Black thick arrows indicate regenerated muscle fibres with centrally placed nuclei. Thin arrow indicates fibrosis. Images are representative of five sections from three mice per genotype. Bar, 50 μm . (D) Percentage of centrally nucleated fibres (CNF) in SOL and TA muscles from 6-w Control, mTORmKO, and mTORmKOKI mice. A minimum of 500 myofibres per SOL muscle and 2800 per TA muscle from three mice per genotype was analysed. (E) Relative mRNA levels of myogenin, IGFII, and MyH8 in SOL muscles from 6-w mTOR mutant mice. Controls ($n = 6$); mTORmKO ($n = 6$); mTORmKOKI ($n = 12$). Data indicate mean \pm SEM. $^*/\#P < 0.05$; $^{**}/###P < 0.01$; $^{***}/####P < 0.001$, * is mTOR mutant vs. Control, $\#$ is mTORmKOKI vs. mTORmKO.

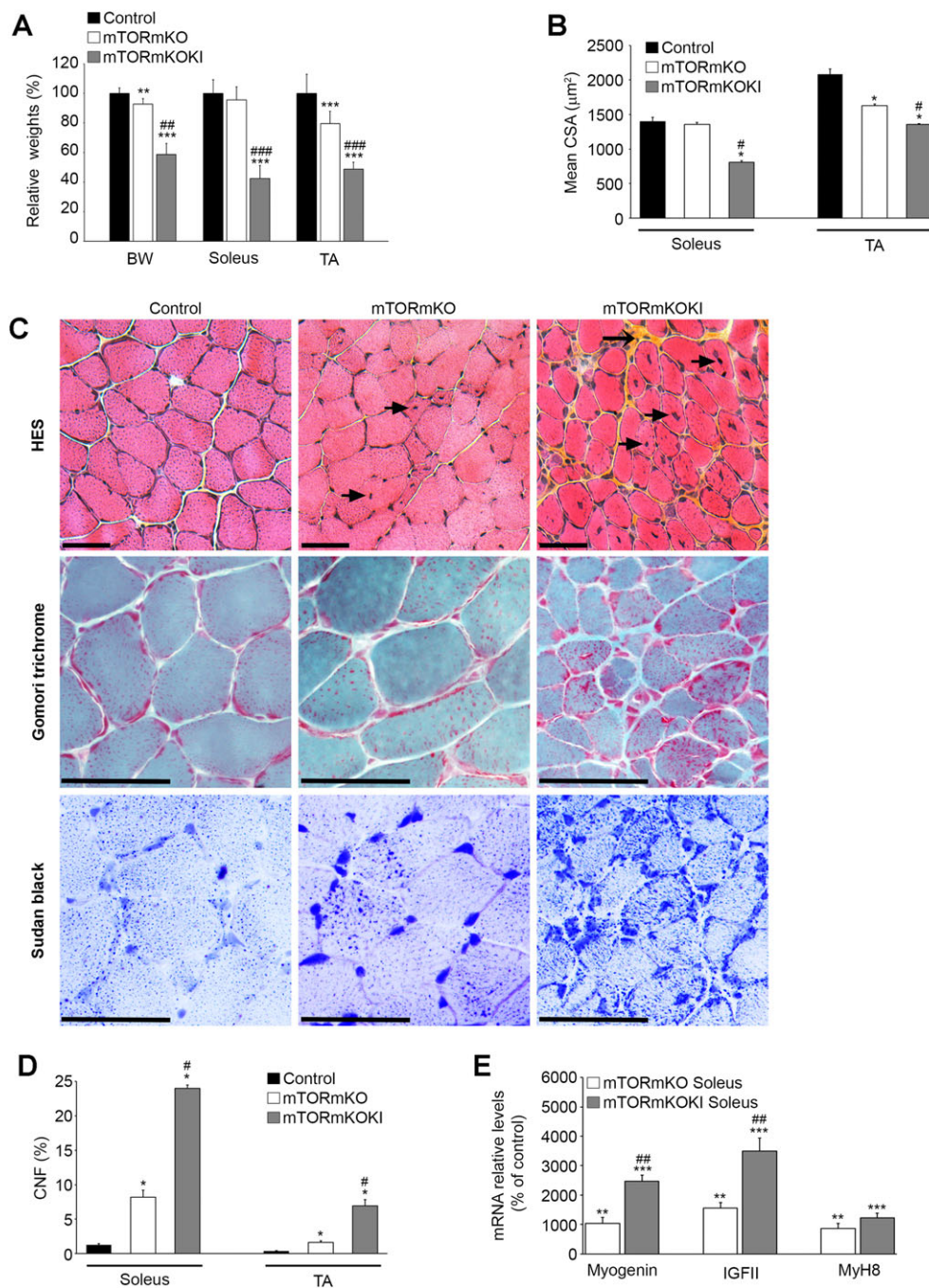
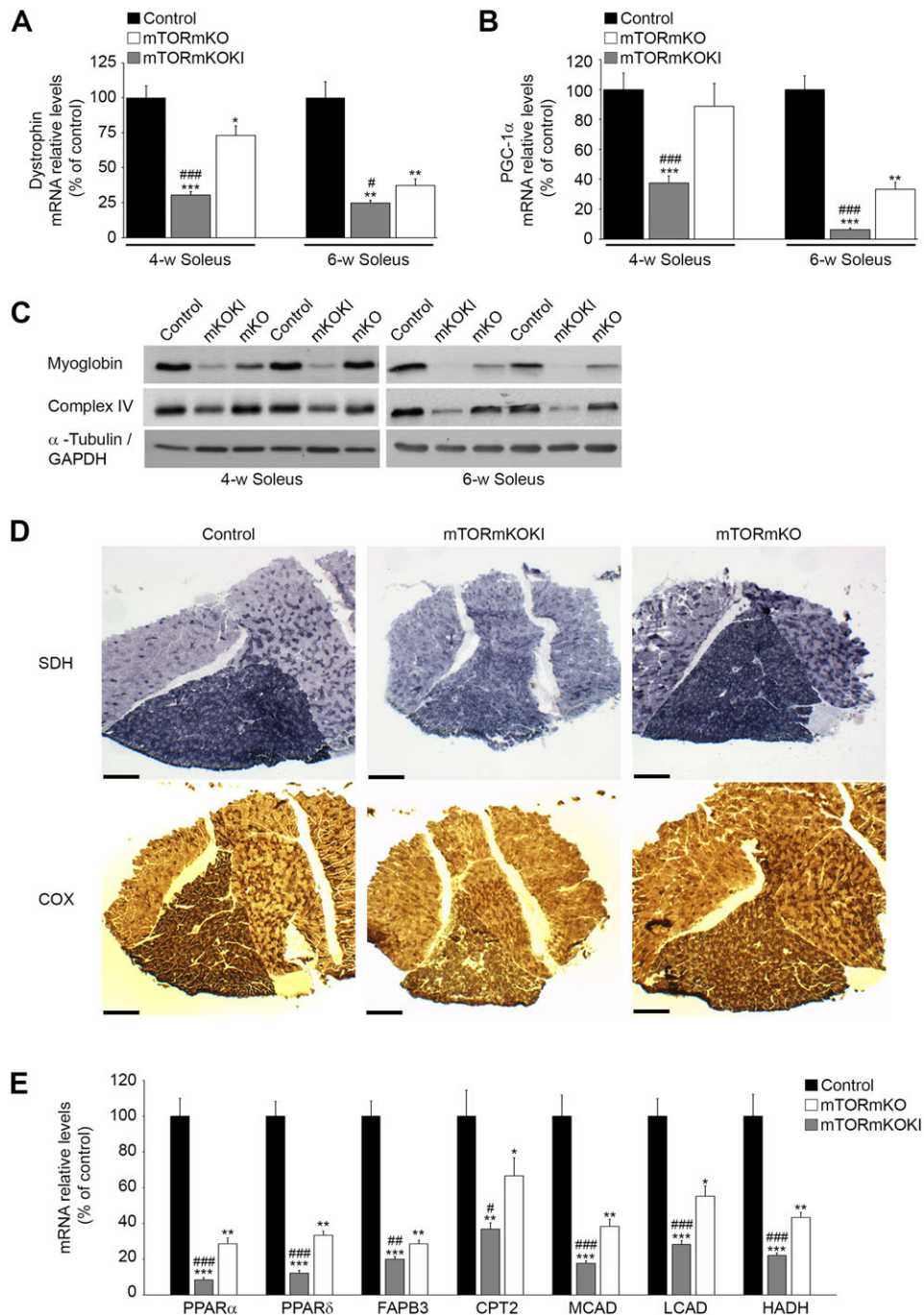


Figure 3 Muscle mTOR kinase activity is required for muscle dystrophin expression and mitochondria function. (A, B) Relative mRNA levels of dystrophin (A) and PGC-1 α (B) in SOL muscles from 4-w Control ($n = 7-13$), mTORMKOI ($n = 8-12$), and mTORMKO ($n = 7-11$) mice, and in SOL muscles from 6-w Control ($n = 6$), mTORMKOI ($n = 6-12$), and mTORMKO ($n = 6$) mice. Data indicate mean \pm SEM. $^{*/\#}P < 0.05$; $^{**/\#\#}P < 0.01$; $^{***/\#\#\#}P < 0.001$, * is mTOR mutant vs. Control, $^\#$ is mTORMKOI vs. mTORMKO. (C) Western blot analysis showing myoglobin and complex IV protein levels in SOL muscle from 4-w and 6-w Control, mTORMKOI, and mTORMKO mice ($n = 3$ mice per age and genotype). α -Tubulin and GAPDH were used as loading control in muscles from 4-w and 6-w mice, respectively. (D) Succinate dehydrogenase (upper panel) and cytochrome oxidase (lower panel) histochemical staining demonstrating defects in the mitochondrial respiratory chain in muscles from 4-w mTORMKOI mice, specifically. Images are representative of five sections from three mice per genotype. Bar, 300 μ m. (E) Relative mRNA levels of PPAR α (peroxisome proliferator-activated receptor- α); PPAR δ (peroxisome proliferator-activated receptor- δ); FABP3 (Fatty-acid-binding protein 3); CPT2 (Carnitine palmitoyltransferase II); MCAD (medium-chain acyl-CoA dehydrogenase); LCAD (long-chain acyl-CoA dehydrogenase); HADH (Hydroxyacyl-Coenzyme A dehydrogenase) in SOL muscles from 6-w control ($n = 5$), mTORMKO ($n = 5$), and mTORMKOI ($n = 10$) mice. Data indicate mean \pm SEM. $^{*/\#}P < 0.05$; $^{**/\#\#}P < 0.01$; $^{***/\#\#\#}P < 0.001$, * is mTOR mutant vs. Control, $^\#$ is mTORMKOI vs. mTORMKO.



Supporting Information, Table S2). In accordance with these results, the intensities of succinate dehydrogenase and cytochrome oxidase staining, indicative of mitochondrial activity, were similar between muscles from 4-w mTORMKO mice and Controls, while strongly reduced in age-matched mTORMKOKI mice (Figure 3D). Defects in muscle mitochondrial energetic activity in mTORMKO mice were consistently observed at 6 weeks of age (Supporting Information, Figure S3). In skeletal muscle, PGC-1 α co-activates the peroxisome proliferator-activated receptors (PPARs), a family of transcription factors that play a key role in mediating mitochondrial biogenesis, oxidative metabolism, and lipid usage.^{33,34} Expression of both PPAR- α and - δ was previously shown to be down-regulated at the mRNA level in muscle from mTORMKO and RAMKO mice.²⁷ To determine whether PPARs expression required mTOR catalytic activity, we examined PPAR- α and - δ transcript levels and we found that they were more down-regulated in mTORMKOKI than mTORMKO muscles (Figure 3E and Supporting Information, Figure S4). Consistently, the expression of PPAR target genes involved in fatty acid uptake and oxidation, such as FABP3, CPT2, MCAD, LCAD, and HADH, was also reduced (Figure 3E and Supporting Information, Figure S4), indicating reduced lipid utilization in mTORMKOKI as compared with mTORMKO skeletal muscle.

Recent studies demonstrated that mitochondrial dysfunction or altered lipid usage leads to induction of the myokine FGF21 (fibroblast growth factor 21) in skeletal muscle of mice and humans as a stress-response to enhance carbohydrate and lipids metabolism.^{35–38} In mice, muscle-derived FGF21 has been linked to leanness^{29,36,38} and smaller body size, possibly through suppression of the IGF1-GH axis.^{39,40} The mitochondrial alterations as well as the phenotype of mTORMKOKI mice suggested a possible involvement of FGF21. However, FGF21 was not induced in skeletal muscle of mTORMKOKI mice (Supporting Information, Figure S5, see also discussion).

Collectively, these data demonstrate that mTOR catalytic activity is essential for the regulation of dystrophin as well as for PPARs/PGC-1 α -mediated regulation of mitochondrial oxidative metabolism and lipid usage in skeletal muscle. In addition, mTORMKOKI mice show clear postnatal anticipation in muscle alterations compared with mTORMKO mice.

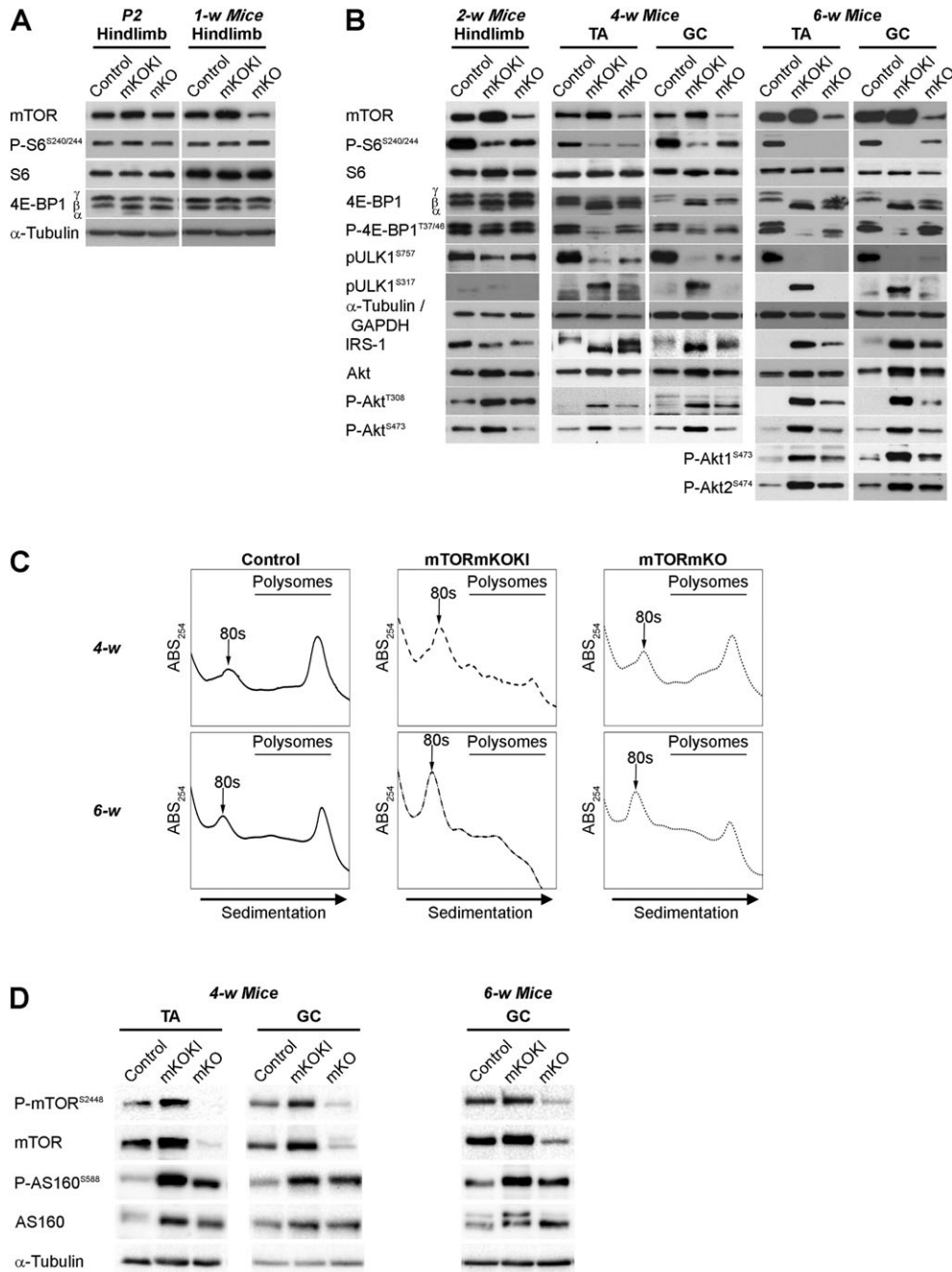
The severe muscle pathological changes in mTORMKOKI mice are due to robust suppression of postnatal mTORC1 signalling

To investigate the mechanisms underlying the exacerbated phenotype of mTORMKOKI, as compared with mTORMKO mice, thorough biochemical analysis of mTOR signalling was performed. mTOR levels in mTORMKO neonates were similar to those in Controls at postnatal day 2 (P2) and progressively decreased at later stage (Figure 4A and 4B). As expected from

HSA promoter-driven expression of the mTOR α protein, total mTOR protein level was up-regulated in postnatal mTORMKOKI muscles. The observation that endogenous murine mTOR mRNA was down-regulated to the same extent in mTORMKOKI and mTORMKO muscles from 2-w mice indicated that mTORMKOKI muscles predominantly expressed the mTOR α protein (Supporting Information, Figure S6). Importantly, muscle mTORC1 signalling remained unaltered in both mutant mouse lines during the first postnatal week (Figure 4A and Supporting Information, Table S2). Normal early postnatal levels of muscle mTOR and mTORC1 signalling in mTOR mutant mice can be attributed to the time needed to recombine the mTOR locus and degrade endogenous mTOR provided by SC nuclei recruited for muscle postnatal growth. Indeed, SC nuclei account for a large proportion of myonuclei within the growing myofibres at this stage.^{13,14} The decrease in the phosphorylation of the mTORC1 targets, S6 ribosomal protein on S240/244, 4E-BP1 on T37/46, and ULK1 on S757 in mutant muscles occurred after the first postnatal week. However, this decrease was remarkably steeper in mTORMKOKI than mTORMKO muscles indicating that suppression of postnatal mTORC1 signalling was robust in mTORMKOKI mice while more progressive in mTORMKO mice (Figure 4B and Supporting Information, Table S2). Moreover, phosphorylation of downstream mTORC1 targets, including S6 and 4E-BP1, was still detectable in muscles from 6-w mTORMKO mice and appeared higher in GC than TA muscles. At this age, this feature can most likely be attributed to muscle regeneration that is prominent in mutant oxidative muscles such as GC, as compared with TA. Indeed, muscle fibre regeneration also involves accretion of SC nuclei and therefore of not yet recombined mTOR locus to muscle fibres. Conversely, mTORC1 signalling was similarly and strongly suppressed in both GC and TA muscles from 6-w mTORMKOKI mice. Altogether, these data indicate that the mTOR α protein exerts a prominent dominant-negative effect on residual endogenous mTOR therefore inducing much more rapid and efficient suppression of mTOR activity in muscle fibres (see discussion).

Finally, the hypophosphorylated 4E-BP1 α isoform was strongly accumulated in muscles from 6-w mTORMKOKI as compared with mTORMKO mice (Figure 4B and Supporting Information, Table S2). Dephosphorylated 4E-BPs have been shown to mediate the largest translation defects caused by mTOR catalytic inhibition.⁴¹ We therefore examined the consequences of the differential accumulation of hypophosphorylated 4E-BPs between mTORMKO and mTORMKOKI GC muscles on translation efficiency in polysome profiling analysis (Figure 4C). In muscle from 4-w and 6-w mTORMKOKI mice, ribosomes were shifted out of polysomes and accumulated as 80s monosomes. Conversely, muscles from 4-w mTORMKO mice still displayed significant amount of active polysomes. The proportion of polysome was decreased at 6 weeks of age, although without reaching

Figure 4 Biochemical characterization of mTOR mutant muscles. (A, B) Hindlimb, TA, and GC muscle extracts from the specified mice at various ages were immunoblotted with the indicated antibodies to examine mTOR signalling ($n = 3$ mice per age and genotype). α -Tubulin was used as loading control in muscles from P2, 1-w, 2-w, and 4-w mice, and GAPDH was used as loading control in muscles from 6-w mice. (C) Representative polysome profiles of GC muscles from 4-w and 6-w Control, mTORMKOKI, and mTORMKO mice fractionated by sucrose density ultracentrifugation as described in the methods section. The concentration of ribosomes was continuously monitored at 254 nm from top to bottom. The monosome peak is marked as 80S. (D) Analysis of the phosphorylation of mTOR at S2448 and AS160 at S588 in mTOR mutant muscles ($n = 3$ mice per age and genotype). α -Tubulin was used as loading control.



the low levels observed in mTORMKOKI muscles. Thus, translation capacities were partially sustained in muscles from mTORMKO mice during juvenile development, while suppressed in mTORMKOKI mice due to enhanced 4E-BPs activity.

Another striking difference between mTORMKOKI and mTORMKO mice was obtained by western blot analysis, which revealed that dephosphorylation of ULK1 on the mTORC1 site S757 was associated with a strong phosphorylation of the AMPK site S317 as soon as 4 weeks of age in

mTORMKOKI muscle. In contrast, ULK1 S317 remained unphosphorylated in muscles from juvenile mTORMKO mice (Figure 4B and Supporting Information, Table S2). Because both the activating phosphorylation of the kinase ULK1 on S317 and active 4E-BP1 in skeletal muscle have been tightly linked to autophagy activation,^{20,42} our observations suggested severely altered autophagy flux in muscles from juvenile mTORMKOKI mice. Altogether, these data indicate that the more severe myopathy of mTORMKOKI as compared with mTORMKO mice is due to more robust suppression of muscle mTORC1 signalling associated with stronger alterations in translation and autophagy during postnatal development.

Finally, we investigated the phosphorylation of mTOR on S2448, a widely used biomarker in the skeletal muscle biology field to assess mTOR activation.⁴³ PKB/Akt has been initially suggested to directly phosphorylate mTOR on this site,^{44,45} while later studies demonstrated that mTOR S2448 is phosphorylated by S6K in a negative feedback loop.^{46,47} Interestingly, phosphorylation of mTOR at S2448 was not abolished but rather increased in muscle from mTORMKOKI as compared with control mice at both 4 and 6 weeks of age, despite inhibition of mTORC1 signalling (Figure 4D and Supporting Information, Table S2). These results demonstrate that inactive muscle mTOR can be phosphorylated at S2448 in a S6K-independent manner, most likely via a mechanism involving PKB/Akt (see below).

mTORMKOKI mice display strong postnatal muscle feedback-mediated PKB α /Akt1 and PKB β /Akt2 activation associated with damaging glycogen accumulation

mTORMKO muscles were previously shown to display increased PKB/Akt activity resulting from (i) alleviation of the mTORC1/S6K-mediated negative feedback loop on the insulin signalling pathway via insulin receptor substrate 1 (IRS1) to PI3K and consequent PDK1-mediated phosphorylation of PKB/Akt T308,²⁸ and (ii) activation of an mTORC2-independent kinase that phosphorylates PKB/Akt on S473.⁹

As expected from more robust mTORC1 signalling suppression, IRS-1 showed stronger downshifted electrophoretic mobility and accumulation in mTORMKOKI muscle (Figure 4B and Supporting Information, Table S2), both being respectively hallmarks of reduced IRS-1 S/T phosphorylation and of decreased proteosomal degradation.^{48,49} Loss of mTORC2 was previously shown to cause accumulation of inactive IRS1 and impaired PKB/Akt activation;⁵⁰ however, phosphorylation of PKB/Akt on both T308 and S473 residues was greater in mTORMKOKI muscles (Figure 4B and Supporting Information, Table S2) indicating enhanced IRS1-PKB/Akt signalling. Interestingly, up-regulation of muscle PKB/Akt S473 phosphorylation started from 2 weeks of age at the latest in mTORMKOKI mice, but after 4 weeks of age in mTORMKO

mice. The ability of PKB/Akt to be phosphorylated on S473 in mTORMKOKI muscle indicates that mTORC2 does not exert dominant effects on the mTORC2-independent kinase for PKB/Akt S473. This observation also demonstrates that activation of the mTORC2-independent kinase in mTOR mutant muscles is a mechanism compensatory to the loss of muscle mTOR kinase activity. Of note, greater phosphorylation of both PKB α /Akt1 S473 and PKB β /Akt2 S474 hydrophobic motifs was found in mTOR mutant muscles (Figure 4B) implying activation of both isoform-specific functions.^{51,52} Previous studies established a major role for IRS-1/Akt2 signalling in insulin-stimulated glucose metabolism in skeletal muscle.^{51,53}

The insulin-regulated Akt substrate Rab GTPase-activating protein TBC1D4/AS160 mediates GLUT4 translocation to the membrane and glucose uptake in muscle cells upon phosphorylation on S588.^{54–57} Consistently with elevated PKB/Akt activity in mTORMKOKI muscle, phosphorylation of S588 on AS160 was greater as compared with mTORMKO and control muscles (Figure 4D and Supporting Information, Table S2), confirming enhanced insulin sensitivity and glucose absorption.

Moreover, analysis of muscle glycogen stores in juvenile mTORMKOKI mice revealed severe alterations in glycogen metabolism, with a 22-fold to 24-fold increase in glycogen content compared with Controls, contrasting with the milder six-fold to eight-fold increase observed in mTORMKO mice (Figure 5A). Electron microscopy of mTORMKOKI muscle showed massive accumulation of densely clustered glycogen granules co-localized with disorganized myofibrils, a feature that was not observed in muscle from age-matched mTORMKO mice (Figure 5B). Thus, it is likely that hyperaccumulation of glycogen in mTORMKOKI muscles damages myofibril organization and contributes to their higher muscle regeneration rates, as compared with mTORMKO muscles (Figure 2 and Supporting Information, Figure S3). The dramatic accumulation of glycogen in mTORMKOKI muscles correlated with very low protein level of the glycogenolysis rate-limiting enzyme, glycogen phosphorylase (GPh), as compared with that in controls and mTORMKO muscles (Figure 5C and Supporting Information, Table S2), thereby demonstrating that mTOR kinase activity is critically required for GPh expression.

We next investigated how the severity of the mTORMKOKI phenotype combined with enhanced muscle insulin signalling affected whole-body glucose homeostasis at 4 weeks of age. As shown in Figure 5D, fed blood glucose levels did not significantly differ between each of mTOR mutant groups and Controls, although they were slightly lower in mTORMKOKI as compared with mTORMKO mice. Serum insulin levels were also similar among the three genotypes (Figure 5E). Glucose tolerance and insulin sensitivity were next analysed after 5 h fasting. Both mTOR mutant mouse lines showed little but significant glucose intolerance as compared with Controls, and this was more pronounced in mTORMKOKI mice

Figure 5 mTORMKOKI mice display massive glycogen accumulation but mild alterations of whole-body glucose homeostasis. (A) Quantification of muscle glycogen content in TA and GC muscles from the indicated mice at 6 weeks of age ($n = 3$ mice per genotype). Results are expressed in μg of glycogen per mg of tissue. (B) Representative electron micrographs of longitudinal section of TA muscles from the indicated mice at 6 weeks of age ($n = 3$ per genotype). Electron micrographs were taken at higher magnifications in mTORMKOKI muscles to visualize the accumulation of glycogen granules. (C) Western blot analysis showing GPh protein levels in TA and GC muscles from 6-w Control and mTOR mutant mice ($n = 3$ mice per genotype). (D) Fed blood glucose levels ($n = 12\text{--}17$ mice per genotype) and (E) fed serum insulin levels ($n = 8\text{--}10$ mice per genotype) in Control and mTOR mutant mice from 4 weeks of age. (F) Glucose tolerance ($n = 9\text{--}11$ mice per genotype) and (G) insulin tolerance ($n = 6\text{--}12$ mice per genotype) tests in 4-w mTOR mutant mice and Controls after 5 h fasting. (F) and (G) Insets show calculated glucose areas under the curve ($\text{AUC}_{0\text{--}120 \text{ min}}$). Data indicate mean \pm SEM. $^*/\#P < 0.05$; $^{**}/\#\#P < 0.01$; $^{***}/\#\#\#P < 0.001$, * is Control vs. mTOR mutant, $\#$ is mTORMKOKI vs. mTORMKO.

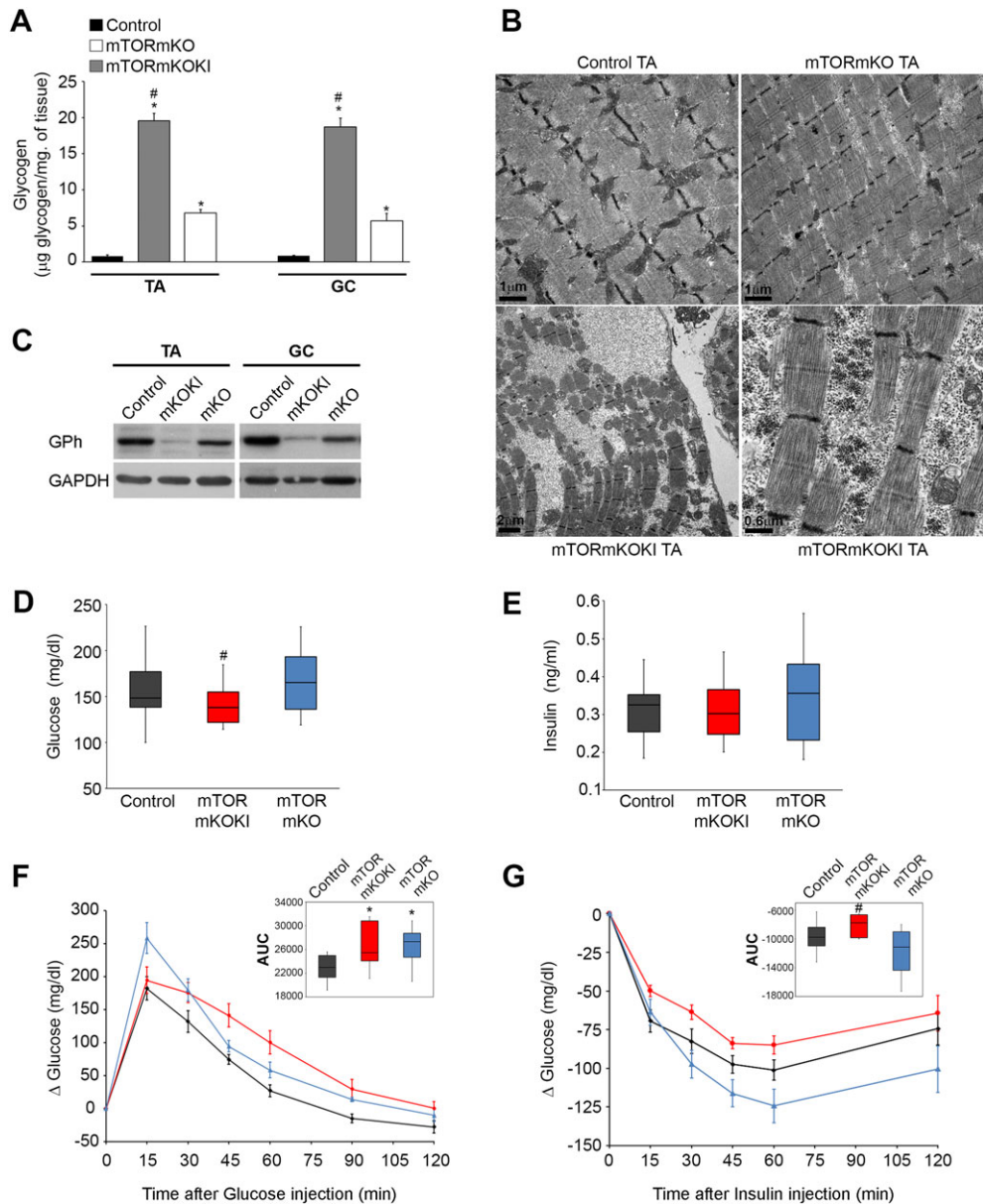


(Figure 5F). Neither mTOR mutant mouse line significantly differed from controls for insulin sensitivity, although mTORMKOKI mice were less sensitive to insulin as compared with mTORMKO mice (Figure 5G).

Discussion

Using loss-of-function mouse models, we and others previously demonstrated a critical role of mTORC1 in muscle

physiology.^{8,9} However, in these studies, the contribution of non-recombined SC during early postnatal muscle growth and regeneration precluded complete elimination of mTORC1 activity in muscle fibres. Here, we examined the consequences of sustained inhibition of mTOR catalytic activity in mouse skeletal muscle. To this aim, we have generated and characterized the mTORMKOKI mouse model that co-expresses an mTOR kinase inactive (mTORki) protein and the Cre recombinase in skeletal muscle fibres carrying an mTOR floxed allele. We find that mTORMKOKI mice develop a much more rapidly progressive and severe myopathy than mTORMKO mice, preventing normal whole-body growth and causing juvenile death. We provide evidence that the severity of the mTORMKOKI as compared with the mild mTORMKO phenotype is due to more robust suppression of muscle mTORC1 signalling.

mTORMKO mice display long lasting postnatal muscle mTORC1 signalling

Our comparative biochemical analysis of muscle from mTORMKOKI and mTORMKO mice revealed long lasting postnatal muscle mTORC1 signalling in mTORMKO mice, allowing persistent oxidative and translational capacities in skeletal muscle during early juvenile development. An explanation for this feature is first provided by the normal muscle mTOR protein content and mTOR signalling in mTOR mutant mice early postnatally. This can be attributed to the time needed to recombine SC nuclei that account for a large proportion of the myonuclei within the growing myofibres at early postnatal stage.^{13,14} In accordance with this, HSA-Cre-mediated targeted gene recombination was shown to display a maximal efficiency around postnatal day 15 (P15).³² Second, mTOR protein levels need to be intensely down-regulated to negatively affect downstream effectors because very low mTOR or raptor levels were shown to maintain mTORC1 signalling. For example, mTOR has to be reduced to less than 25% its normal level in cells to observe any effect on S6K1 phosphorylation.^{58,59} In addition, mTOR heterozygous mice display unaltered S6 and 4EBP phosphorylation levels,⁶⁰ while mice with a constitutive 75% reduction of mTOR protein levels exhibit a decrease, but not a suppression, in mTORC1 signalling without changes in overall protein translation.⁶¹ In line with this, phosphorylated substrates of mTORC1 could be detected in muscle from 6-w mTORMKO mice despite the low mTOR content. Moreover, down-regulation of mTORC1 signalling in mTOR-depleted muscle fibres is further dependent on mTOR targets turnover as well as the effect of phosphatases. Finally, loss of mTORC1-mediated functions in mTORMKO muscles must await for the dephosphorylation events to be translated at other molecular and cellular levels (e.g. gene transcription and translation, and ribosome

content). As stated earlier, muscles from 6-w mTORMKO mice show residual phosphorylation of mTORC1 targets, which appeared higher in the oxidative GC muscle as compared with the glycolytic TA muscle. At this age, this can be explained by the higher levels of regeneration of oxidative mTOR mutant muscle, a process which, similar to the early postnatal fibre growth phase, involves the accretion of non-recombined SC nuclei.¹⁵ Consequently, we hypothesize that mTOR activity provided by SC to mTORMKO muscle during early postnatal muscle growth and regeneration is sufficient to support initial muscle growth and function. The mass preservation of the oxidative slow-twitch SOL in mTORMKO mice at least until 6 weeks of age is particularly remarkable. This protection might possibly be conferred by greater SC nuclei contribution during early postnatal growth and regeneration. Indeed, SC content is known to be much higher in slow-twitch than fast-twitch muscles.⁶²

The kinase inactive mTOR mutant protein induces robust suppression of postnatal muscle mTORC1 signalling in mTORMKO mice

Efficient suppression of mTOR activity in mTORMKOKI muscle implies that the mTORki protein exerts dominant-negative effects on residual mTOR present in mTORMKO muscle fibres. Several lines of evidence indicate that the ability of the mutant mTORki to exert dominant negative activity depends on the relative abundance of mutant vs. wildtype mTOR protein. For example, an mTORki/mTORwt ratio of 2 to 3 in skeletal muscle from mTORMKI transgenic mice was shown to be insufficient to affect the phosphorylation of mTORC1 substrates and did not lead to any obvious phenotype.¹² Likewise, mTOR+/mTORki heterozygous mice display wildtype mTOR activity in tissues.⁶³ While an mTORki/mTORwt ratio of 4 to 6 in cardiac muscle from transgenic mice was sufficient to alter mTORC1 signalling,⁶⁴ it did not cause the severe phenotype of cardiac muscle-specific mTOR knockout mice.³¹ Similarly, transgenic mice exhibiting an mTORki/mTORwt ratio of 2 to 3 in β -cells produced a mild down-regulation of mTOR signalling,⁶⁵ although without affecting the mass of β -cell as observed in β -cell specific Raptor knockout mice.⁶⁶ Conversely, our strategy combining mTORki expression during the course of postnatal mTOR inactivation in skeletal muscle from mTORMKOKI mice allowed to achieve a robust suppression of mTORC1 activity associated with earlier and stronger alterations in protein synthesis and metabolism as compared with mTORMKO muscles. In addition, the strong phosphorylation of ULK1 on S317 and accumulation of unphosphorylated 4EBP are specific to muscles from juvenile mTORMKOKI mice and indicate impaired autophagy.^{20,42} This feature may exacerbate the myopathy of mTORMKOKI mice.⁶⁷

mTOR catalytic activity is required for oxidative metabolism and dystrophin expression

Kinase-dependent and kinase-independent functions of mTOR have been shown to control skeletal muscle development.³⁰ The presence of fibres with nuclear centralization in mTORMKOKI mice supports previous findings indicating that muscle regeneration *in vivo* can be initiated independently of mTOR kinase activity.¹² Several reports show that mTORC1 activity regulates PGC-1 α and oxidative metabolism.^{22–24} The down-regulation of oxidative metabolism as well as expression of PPARs and PGC-1 α in mTORMKOKI muscles demonstrates that mTOR catalytic activity is required for these regulations *in vivo*. Conversely, dystrophin expression was previously shown to be independent of mTOR kinase activity.⁹ However, mTORMKOKI muscles showed a marked reduction in dystrophin expression. This discrepancy might result from differences between acute overexpression of the mTOR ki mutant by electroporation⁹ and sustained HSA-driven mTOR ki mutant expression in mTORMKOKI mice (this study). Moreover, mTORMKOKI muscles are much more atrophic and regenerating as compared with the previously electroporated mTORMKO muscles. Fiorillo *et al.* recently published pathological contexts in which muscle atrophy and regeneration are associated with inflammatory pathways inducing down-regulation of dystrophin via dystrophin-targeting miRNA.⁶⁸ Such mechanisms may therefore mask dystrophin activation by the mTOR ki mutant protein.

Juvenile mTORMKOKI mice show features of glycogenosis and mild alterations of whole-body glucose homeostasis

PKB/Akt activation in muscles from juvenile mTORMKOKI mice is associated with a remarkable down-regulation of GPh, the enzyme catalysing glycogen breakdown, and with overwhelming accumulation of muscle glycogen. Electronic microscopy shows complete disorganization of the contractile apparatus at the glycogen accumulation sites of mTORMKOKI fibres specifically. Such glycogen accumulation was not reported in muscles from distinct transgenic mouse models expressing constitutively active PKB α /Akt1.^{69–71} Feedback-mediated activation of both Akt1 and Akt2 specific-functions^{51,52} is thus likely required to develop the glycogen phenotype of mTOR mutant muscles. Altogether, our data indicate that early postnatal inhibition of muscle mTOR activity causes glycogen storage disease type V (also called McArdle disease)-like phenotype. Indeed, the alterations related to glycogen accumulation in juvenile mTORMKOKI mice resemble features of the murine model of McArdle disease that is deficient in GPh.⁷² In this model, glycogen accumulation is also associated with muscle regeneration.⁷³ Moreover, muscle from these mice shows AMPK activation⁷⁴ suggesting that AMPK-dependent

phosphorylation of ULK1 S317 in mTORMKOKI muscles might be a consequence of altered glycogen metabolism. Despite enhanced muscle insulin signalling, as indicated by activation of Akt/PKB and AS160, young mTORMKOKI mice display mild decreased glucose and insulin tolerance. Because skeletal muscle and adipose tissue accounts for, respectively, about 70% and 10% of insulin-mediated glucose uptake,⁷⁵ altered whole-body glucose homeostasis in mTORMKOKI mice most likely results from their pronounced reduction in muscle and fat mass. These alterations might reflect the onset of myopathy-associated metabolic complications that were observed in aged RAMKO mice.⁷⁶

Catalytic activity of muscle mTOR is required for whole-body postnatal growth

The small size of organs in mTORMKOKI mice demonstrates the importance of mTOR catalytic activity within skeletal muscle for whole-body postnatal growth. This period of life is highly demanding in energy¹³ and skeletal muscle is known to influence energy and protein metabolism throughout the body.⁷⁷ mTORMKOKI muscles are likely unable to provide peripheral organs with sufficient energy and substrates to allow their growth,^{78–80} while simultaneously acting as a glucose sink at the expense of other tissues as discussed in Albert and Hall.² In addition, we cannot rule out the possible influence of muscle-secreted myokines contributing to the lean and small mTORMKOKI phenotype. In this sense, mTORMKO mice have been shown to induce the myokine Serpina3.⁸¹ Nevertheless, the FGF21 myokine is not involved despite mTORMKOKI mice exhibit features known to up-regulate muscle-derived FGF21, including mitochondria dysfunction,^{35,36,39,40} impaired lipid usage,^{37,38} and activated PKB/Akt.⁸² It is tempting to speculate that mTORMKOKI muscles are mechanically unable to induce FGF21. In support of this notion, FGF21 has been shown to be under mTORC1 control because its transcriptional induction is rapamycin-sensitive^{29,83–85} and is directly mediated by transcription factors themselves regulated by mTOR, such as PPARs, ATF4, and ChREBP.^{86–89}

Collectively, our results reveal a heretofore unappreciated role of muscle mTOR catalytic activity in the regulation of whole-body homeostasis. Our study provides new evidence for the dramatic consequences that can be induced by dysregulation of muscle mTOR signalling and suggests that skeletal muscle targeting with mTOR catalytic inhibitors may have detrimental effects.

Acknowledgements

We acknowledge the contribution of the animal facility (AniRA PBES) and the imaging facility (LBI-PLATIM) of the

SFR biosciences (UMS3444/CNRS, US8/Inserm, ENS de Lyon, UCBL). We thank Elisabeth Errazuriz-Cerda (CIQLE, Lyon) for help in electron microscopy, Daniel Taillandier for help with polysome profile analysis, Véronique Morel and Gaël Yvert for help with the statistical analysis, and Pascal Leblanc for critical reading of the manuscript. The authors certify that they comply with the ethical guidelines for authorship and publishing in the Journal of Cachexia, Sarcopenia, and Muscle.⁹⁰ The manuscript does not contain clinical studies or patient data.

Conflict of interest

None declared.

Funding

This work was supported by National Natural Science Foundation of China (grant no. 31171142), China Scholarship Council, CMIRA, ENS of Lyon, Suzhou Municipal Bureau of Science and Technology (SYS201711) (to Q.Z.), NIH R01 AR048914 (to J.C.), the Association Française contre les Myopathies (to L.S., and Y.-G.G.) and MyoNeurALP alliance.

Online supplementary material

Additional supporting information may be found online in the Supporting Information section at the end of the article.

Figure S1. Histogram showing distributions of myofiber CSA in SOL (A) and TA (B) muscles from 6-w control and mTOR mutant mice. This analysis includes a minimum of 400 myofibers per SOL muscle and 1200 myofibers per TA muscle from three mice per genotype. Data indicate mean \pm SEM.

Figure S2. Examination of the muscle dystrophy from mTOR mutant mice. (A) Number of peripheral myonuclei per fiber section in TA muscle from 3-w mice. Cross sections were immunostained with WGA (green) and Dapi (red). Fiber myonuclei are defined by having the mass center of the Dapi stain inside the WGA ring. Examples of peripheral myonuclei are indicated by an arrow and external nuclei by an arrowhead. The number of myonuclei per transverse section is indicated below each panel. Data indicate mean \pm SEM for 3 mice per group, two cross sections each and 200 fibers per section. Bar, 25 μ m. (B) Representative HE staining of TA muscle sections from 6-w Control, mTORMKO and mTORMKOKI mice. Black arrows indicate re-generated muscle fibers with centrally placed nuclei. Bar, 50 μ m. (C) Relative mRNA levels of myogenin, IGFII and

MyH8 in TA muscles from 6-w mTOR mutant mice. Controls ($n = 6$); mTORMKO ($n = 6$); mTORMKOKI ($n = 6$). (D) Relative mRNA levels of myogenin, IGFII and MyH8 in EDL muscles from 6-w mTOR mutant mice. Controls ($n = 6$); mTORMKO ($n = 7$); mTORMKOKI ($n = 5$). (E) Hematoxylin & Eosin & Saffron (left panel) and Sudan black (right panel) stainings of soleus muscle sections from 6-w mTORMKOKI mice showing adipose infiltration (Black arrows). Data indicate mean \pm SEM. */# $P < 0.05$; **/### $P < 0.01$; ***/#### $P < 0.001$, * is mTOR mutant vs. Control, # is mTORMKOKI vs. mTORMKO.

Figure S3. Visualization of mitochondrial respiratory function in muscles from 6-w control and mTOR mutant mice. (A) Succinate dehydrogenase (SDH) staining; Bar, 200 μ m. (B) Cytochrome oxidase (COX) staining; Bar, 300 μ m.

Figure S4. Decreased expression of genes involved in fatty acid transport and oxidation in skeletal muscle from 6-w control and mTOR mutant mice. Relative mRNA levels of PPAR α (peroxisome proliferator-activated receptor- α); PPAR δ (peroxisome proliferator-activated receptor- δ); FABP3 (Fatty-acid-binding protein 3); CPT2 (Carnitine palmitoyltransferase II); MCAD (medium-chain acyl-CoA dehydrogenase); LCAD (long-chain acyl-CoA dehydrogenase); HADH (Hydroxyacyl-Coenzyme A dehydrogenase) in TA muscles from control ($n = 5$), mTORMKO ($n = 5$) and mTORMKOKI ($n = 10$) mice. Data indicate mean \pm SEM. */# $P < 0.05$; **/### $P < 0.01$; ***/#### $P < 0.001$, * is mTOR mutant vs. Control, # is mTORMKOKI vs. mTORMKO.

Figure S5. Muscle FGF21 is not induced in mTORMKOKI mice. (A) FGF21 protein levels in GC muscle from 4-w control and mTOR mutant mice ($n = 3$ mice per genotype); (B) Relative mRNA levels of FGF21 in SOL muscle from 6-w control ($n = 5$), mTORMKO ($n = 7$) and mTORMKOKI ($n = 5$) mice. Data indicate mean \pm SEM.

Figure S6. Efficient recombination of the mTOR floxed gene in skeletal muscle from mTOR mutant mice. Relative mouse mTOR mRNA levels in muscle from control ($n = 8$), mTORMKO ($n = 6$) and mTORMKOKI ($n = 6$) mice at two weeks of age. Data indicate mean \pm SEM. *** $P < 0.001$, * is mTOR mutant vs. Control.

Table S1. Nomenclature and specificities of muscle mTOR mouse models. This table lists all the mTOR mouse models used in this study by name and genotype, identifying knockout of the endogenous mTOR floxed gene and/or overexpression of either FLAG-mTOR kinase inactive protein or FLAG-mTOR wildtype protein, and describing the specificity of the models.

Table S2. Quantification of Western-blot analysis for the indicated proteins. Numbers represent mean quantification values \pm SEM after subtraction of the background. Number of replicates represents the number of animals per genotype analyzed. A two-tailed Student's *t* test was used for statistical analysis. Abbreviation: N/A, Not Applicable. # $P < 0.05$; ## $P < 0.01$; # is mTORMKOKI vs. mTORMKO.

References

- Schiaffino S, Dyar KA, Ciciliot S, Blaauw B, Sandri M. Mechanisms regulating skeletal muscle growth and atrophy. *FEBS J* 2013;**280**:4294–4314.
- Albert V, Hall MN. mTOR signaling in cellular and organismal energetics. *Curr Opin Cell Biol* 2015;**33**:55–66.
- Jacinto E, Loewith R, Schmidt A, Lin S, Ruegg MA, Hall A, et al. Mammalian TOR complex 2 controls the actin cytoskeleton and is rapamycin insensitive. *Nat Cell Biol* 2004;**6**:1122–1128.
- Sarbassov DD, Ali SM, Sengupta S, Sheen JH, Hsu PP, Bagley AF, et al. Prolonged rapamycin treatment inhibits mTORC2 assembly and Akt/PKB. *Mol Cell* 2006;**22**:159–168.
- Bodine SC, Stitt TN, Gonzalez M, Kline WO, Stover GL, Bauerlein R, et al. Akt/mTOR pathway is a crucial regulator of skeletal muscle hypertrophy and can prevent muscle atrophy in vivo. *Nat Cell Biol* 2001;**3**:1014–1019.
- Pallafacchina G, Calabria E, Serrano AL, Kalhovde JM, Schiaffino S. A protein kinase B-dependent and rapamycin-sensitive pathway controls skeletal muscle growth but not fiber type specification. *Proc Natl Acad Sci U S A* 2002;**99**:9213–9218.
- Goodman CA, Frey JW, Mabrey DM, Jacobs BL, Lincoln HC, You JS, et al. The role of skeletal muscle mTOR in the regulation of mechanical load-induced growth. *J Physiol* 2011;**589**:5485–5501.
- Bentzinger CF, Romanino K, Cloetta D, Lin S, Mascarenhas JB, Oliveri F, et al. Skeletal muscle-specific ablation of raptor, but not of rictor, causes metabolic changes and results in muscle dystrophy. *Cell Metab* 2008;**8**:411–424.
- Risson V, Mazelin L, Rocerì M, Sanchez H, Moncollin V, Corneloup C, et al. Muscle inactivation of mTOR causes metabolic and dystrophin defects leading to severe myopathy. *J Cell Biol* 2009;**187**:859–874.
- Kumar A, Harris TE, Keller SR, Choi KM, Magnuson MA, Lawrence JC Jr. Muscle-specific deletion of rictor impairs insulin-stimulated glucose transport and enhances Basal glycogen synthase activity. *Mol Cell Biol* 2008;**28**:61–70.
- Bodine SC. mTOR signaling and the molecular adaptation to resistance exercise. *Med Sci Sports Exerc* 2006;**38**:1950–1957.
- Ge Y, Wu AL, Warnes C, Liu J, Zhang C, Kawasome H, et al. mTOR regulates skeletal muscle regeneration in vivo through kinase-dependent and kinase-independent mechanisms. *Am J Physiol Cell Physiol* 2009.
- White RB, Bierinx AS, Gnocchi VF, Zammit PS. Dynamics of muscle fibre growth during postnatal mouse development. *BMC Dev Biol* 2010;**10**:21.
- Hawke TJ, Garry DJ. Myogenic satellite cells: physiology to molecular biology. *J Appl Physiol* 2001;**91**:534–551.
- Yin H, Price F, Rudnicki MA. Satellite cells and the muscle stem cell niche. *Physiol Rev* 2013;**93**:23–67.
- Nicole S, Desforges B, Millet G, Lesbordes J, Cifuentes-Diaz C, Vertes D, et al. Intact satellite cells lead to remarkable protection against Smn gene defect in differentiated skeletal muscle. *J Cell Biol* 2003;**161**:571–582.
- Castets P, Lin S, Rion N, Di Fulvio S, Romanino K, Guridi M, et al. Sustained activation of mTORC1 in skeletal muscle inhibits constitutive and starvation-induced autophagy and causes a severe, late-onset myopathy. *Cell Metab* 2013;**17**:731–744.
- Saxton RA, Sabatini DM. mTOR Signaling in Growth, Metabolism, and Disease. *Cell* 2017;**169**:361–371.
- Ohanna M, Sobering AK, Lapointe T, Lorenzo L, Praud C, Petroulakis E, et al. Atrophy of S6K1(-/-) skeletal muscle cells reveals distinct mTOR effectors for cell cycle and size control. *Nat Cell Biol* 2005;**7**:286–294.
- Tsai S, Sitzmann JM, Dastidar SG, Rodriguez AA, Vu SL, McDonald CE, et al. Muscle-specific 4E-BP1 signaling activation improves metabolic parameters during aging and obesity. *J Clin Invest* 2015;**125**:2952–2964.
- Kim YC, Guan KL. mTOR: a pharmacologic target for autophagy regulation. *J Clin Invest* 2015;**125**:25–32.
- Cunningham JT, Rodgers JT, Arlow DH, Vazquez F, Mootha VK, Puigserver P. mTOR controls mitochondrial oxidative function through a YY1-PGC-1 α transcriptional complex. *Nature* 2007;**450**:736–740.
- Blattler SM, Verduguer F, Liesa M, Cunningham JT, Vogel RO, Chim H, et al. Defective mitochondrial morphology and bioenergetic function in mice lacking the transcription factor Yin Yang 1 in skeletal muscle. *Mol Cell Biol* 2012;**32**:3333–3346.
- Morita M, Gravel SP, Chenard V, Sikstrom K, Zheng L, Alain T, et al. mTORC1 controls mitochondrial activity and biogenesis through 4E-BP-dependent translational regulation. *Cell Metab* 2013;**18**:698–711.
- Bentzinger CF, Lin S, Romanino K, Castets P, Guridi M, Summermatter S, et al. Differential response of skeletal muscles to mTORC1 signaling during atrophy and hypertrophy. *Skelet Muscle* 2013;**3**:6.
- Handschin C, Chin S, Li P, Liu F, Maratos-Flier E, Lebrasseur NK, et al. Skeletal muscle fiber-type switching, exercise intolerance, and myopathy in PGC-1 α muscle-specific knock-out animals. *J Biol Chem* 2007;**282**:30014–30021.
- Romanino K, Mazelin L, Albert V, Conjard-Duplany A, Lin S, Bentzinger CF, et al. Myopathy caused by mammalian target of rapamycin complex 1 (mTORC1) inactivation is not reversed by restoring mitochondrial function. *Proc Natl Acad Sci U S A* 2011;**108**:20808–20813.
- Um SH, D'Alessio D, Thomas G. Nutrient overload, insulin resistance, and ribosomal protein S6 kinase 1, S6K1. *Cell Metab* 2006;**3**:393–402.
- Guridi M, Tintignac LA, Lin S, Kupr B, Castets P, Ruegg MA. Activation of mTORC1 in skeletal muscle regulates whole-body metabolism through FGF21. *Sci Signal* 2015;**8**:ra113.
- Ge Y, Chen J. Mammalian target of rapamycin (mTOR) signaling network in skeletal myogenesis. *J Biol Chem* 2012;**287**:43928–43935.
- Mazelin L, Panthu B, Nicot AS, Belotti E, Tintignac L, Teixeira G, et al. mTOR inactivation in myocardium from infant mice rapidly leads to dilated cardiomyopathy due to translation defects and p53/JNK-mediated apoptosis. *J Mol Cell Cardiol* 2016;**97**:213–225.
- Cifuentes-Diaz C, Frugier T, Tiziano FD, Lacene E, Roblot N, Joshi V, et al. Deletion of murine SMN exon 7 directed to skeletal muscle leads to severe muscular dystrophy. *J Cell Biol* 2001;**152**:1107–1114.
- Luquet S, Lopez-Soriano J, Holst D, Fredenrich A, Melki J, Rassoulzadegan M, et al. Peroxisome proliferator-activated receptor delta controls muscle development and oxidative capability. *FASEB J* 2003;**17**:2299–2301.
- Finck BN, Bernal-Mizrachi C, Han DH, Coleman T, Sambandam N, LaRiviere LL, et al. A potential link between muscle peroxisome proliferator-activated receptor- α signaling and obesity-related diabetes. *Cell Metab* 2005;**1**:133–144.
- Lehtonen JM, Forsstrom S, Bottani E, Viscomi C, Baris OR, Isoniemi H, et al. FGF21 is a biomarker for mitochondrial translation and mtDNA maintenance disorders. *Neurology* 2016;**87**:2290–2299.
- Kim KH, Jeong YT, Kim SH, Jung HS, Park KS, Lee HY, et al. Metformin-induced inhibition of the mitochondrial respiratory chain increases FGF21 expression via ATF4 activation. *Biochem Biophys Res Commun* 2013;**440**:76–81.
- Harris LA, Skinner JR, Shew TM, Pietka TA, Abumrad NA, Wolins NE. Perilipin 5-Driven Lipid Droplet Accumulation in Skeletal Muscle Stimulates the Expression of Fibroblast Growth Factor 21. *Diabetes* 2015;**64**:2757–2768.
- Vandanmagsar B, Warfel JD, Wicks SE, Ghosh S, Salbaum JM, Burk D, et al. Impaired Mitochondrial Fat Oxidation Induces FGF21 in Muscle. *Cell Rep* 2016;**15**:1686–1699.
- Keipert S, Ost M, Johann K, Imber F, Jastroch M, van Schothorst EM, et al. Skeletal muscle mitochondrial uncoupling drives endocrine cross-talk through the induction of FGF21 as a myokine. *Am J Physiol Endocrinol Metab* 2014;**306**:E469–E482.
- Tezze C, Romanello V, Desbats MA, Fadini GP, Albiro M, Favaro G, et al. Age-Associated Loss of OPA1 in Muscle Impacts Muscle Mass, Metabolic Homeostasis, Systemic Inflammation, and Epithelial Senescence. *Cell Metab* 2017;**25**:1374–1389, e6.
- Thoreen CC, Chantranupong L, Keys HR, Wang T, Gray NS, Sabatini DM. A unifying model for mTORC1-mediated regulation of mRNA translation. *Nature* 2012;**485**:109–113.

42. Kim J, Kundu M, Viollet B, Guan KL. AMPK and mTOR regulate autophagy through direct phosphorylation of Ulk1. *Nat Cell Biol* 2011;**13**:132–141.
43. Figueiredo VC, Markworth JF, Cameron-Smith D. Considerations on mTOR regulation at serine 2448: implications for muscle metabolism studies. *Cell Mol Life Sci* 2017;**74**:2537–2545.
44. Nave BT, Ouwens M, Withers DJ, Alessi DR, Shepherd PR. Mammalian target of rapamycin is a direct target for protein kinase B: identification of a convergence point for opposing effects of insulin and amino-acid deficiency on protein translation. *Biochem J* 1999;**344**:427–431.
45. Sekulic A, Hudson CC, Homme JL, Yin P, Otterness DM, Karnitz LM, et al. A direct linkage between the phosphoinositide 3-kinase-AKT signaling pathway and the mammalian target of rapamycin in mitogen-stimulated and transformed cells. *Cancer Res* 2000;**60**:3504–3513.
46. Holz MK, Blenis J. Identification of S6 kinase 1 as a novel mammalian target of rapamycin (mTOR)-phosphorylating kinase. *J Biol Chem* 2005;**280**:26089–26093.
47. Chiang GG, Abraham RT. Phosphorylation of mammalian target of rapamycin (mTOR) at Ser-2448 is mediated by p70S6 kinase. *J Biol Chem* 2005;**280**:25485–25490.
48. Pederson TM, Kramer DL, Rondinone CM. Serine/threonine phosphorylation of IRS-1 triggers its degradation: possible regulation by tyrosine phosphorylation. *Diabetes* 2001;**50**:24–31.
49. Ge Y, Yoon MS, Chen J. Raptor and Rheb negatively regulate skeletal myogenesis through suppression of insulin receptor substrate 1 (IRS1). *J Biol Chem* 2011;**286**:35675–35682.
50. Kim SJ, DeStefano MA, Oh WJ, Wu CC, Vega-Cotto NM, Finlan M, et al. mTOR complex 2 regulates proper turnover of insulin receptor substrate-1 via the ubiquitin ligase subunit Fbw8. *Mol Cell* 2012;**48**:875–887.
51. Bouzakri K, Zachrisson A, Al-Khalili L, Zhang BB, Koistinen HA, Krook A, et al. siRNA-based gene silencing reveals specialized roles of IRS-1/Akt2 and IRS-2/Akt1 in glucose and lipid metabolism in human skeletal muscle. *Cell Metab* 2006;**4**:89–96.
52. Cleasby ME, Reinten TA, Cooney GJ, James DE, Kraegen EW. Functional studies of Akt isoform specificity in skeletal muscle in vivo; maintained insulin sensitivity despite reduced insulin receptor substrate-1 expression. *Mol Endocrinol* 2007;**21**:215–228.
53. Hajdich E, Litherland GJ, Hundal HS. Protein kinase B (PKB/Akt)—a key regulator of glucose transport? *FEBS Lett* 2001;**492**:199–203.
54. Sano H, Kane S, Sano E, Miinea CP, Asara JM, Lane WS, et al. Insulin-stimulated phosphorylation of a Rab GTPase-activating protein regulates GLUT4 translocation. *J Biol Chem* 2003;**278**:14599–14602.
55. Randhawa VK, Ishikura S, Talior-Volodarsky I, Cheng AW, Patel N, Hartwig JH, et al. GLUT4 vesicle recruitment and fusion are differentially regulated by Rac, AS160, and Rab8A in muscle cells. *J Biol Chem* 2008;**283**:27208–27219.
56. Stockli J, Davey JR, Hohnen-Behrens C, Xu A, James DE, Ramm G. Regulation of glucose transporter 4 translocation by the Rab guanine triphosphatase-activating protein AS160/TBC1D4: role of phosphorylation and membrane association. *Mol Endocrinol* 2008;**22**:2703–2715.
57. Sakamoto K, Holman GD. Emerging role for AS160/TBC1D4 and TBC1D1 in the regulation of GLUT4 traffic. *Am J Physiol Endocrinol Metab* 2008;**295**:E29–E37.
58. Kim DH, Sarbassov DD, Ali SM, King JE, Latek RR, Erdjument-Bromage H, et al. mTOR interacts with raptor to form a nutrient-sensitive complex that signals to the cell growth machinery. *Cell* 2002;**110**:163–175.
59. Breuleux M, Klopfenstein M, Stephan C, Doughy CA, Barys L, Maira SM, et al. Increased AKT S473 phosphorylation after mTORC1 inhibition is rictor dependent and does not predict tumor cell response to PI3K/mTOR inhibition. *Mol Cancer Ther* 2009;**8**:742–753.
60. Lang CH, Frost RA, Bronson SK, Lynch CJ, Vary TC. Skeletal muscle protein balance in mTOR heterozygous mice in response to inflammation and leucine. *Am J Physiol Endocrinol Metab* 2010;**298**:E1283–E1294.
61. Wu JJ, Liu J, Chen EB, Wang JJ, Cao L, Narayan N, et al. Increased mammalian lifespan and a segmental and tissue-specific slowing of aging after genetic reduction of mTOR expression. *Cell Rep* 2013;**4**:913–920.
62. Gibson MC, Schultz E. Age-related differences in absolute numbers of skeletal muscle satellite cells. *Muscle Nerve* 1983;**6**:574–580.
63. Shor B, Cavender D, Harris C. A kinase-dead knock-in mutation in mTOR leads to early embryonic lethality and is dispensable for the immune system in heterozygous mice. *BMC Immunol* 2009;**10**:28.
64. Shen WH, Chen Z, Shi S, Chen H, Zhu W, Penner A, et al. Cardiac restricted overexpression of kinase-dead mammalian target of rapamycin (mTOR) mutant impairs the mTOR-mediated signaling and cardiac function. *J Biol Chem* 2008;**283**:13842–13849.
65. Alejandro EU, Bozadjieva N, Blandino-Rosano M, Wasan MA, Elghazi L, Vadrevu S, et al. Overexpression of Kinase-Dead mTOR Impairs Glucose Homeostasis by Regulating Insulin Secretion and Not beta-Cell Mass. *Diabetes* 2017;**66**:2150–2162.
66. Blandino-Rosano M, Barbaresso R, Jimenez-Palomares M, Bozadjieva N, Werneck-de-Castro JP, Hatanaka M, et al. Loss of mTORC1 signalling impairs beta-cell homeostasis and insulin processing. *Nat Commun* 2017;**8**:16014.
67. Bonaldo P, Sandri M. Cellular and molecular mechanisms of muscle atrophy. *Dis Model Mech* 2013;**6**:25–39.
68. Fiorillo AA, Heier CR, Novak JS, Tully CB, Brown KJ, Uaesoontrachoon K, et al. TNF-alpha-Induced microRNAs Control Dystrophin Expression in Becker Muscular Dystrophy. *Cell Rep* 2015;**12**:1678–1690.
69. Lai KM, Gonzalez M, Poueymirou WT, Kline WO, Na E, Zlotchenko E, et al. Conditional activation of akt in adult skeletal muscle induces rapid hypertrophy. *Mol Cell Biol* 2004;**24**:9295–9304.
70. Mammucari C, Milan G, Romanello V, Masiero E, Rudolf R, Del Piccolo P, et al. FoxO3 controls autophagy in skeletal muscle in vivo. *Cell Metab* 2007;**6**:458–471.
71. Izumiya Y, Hopkins T, Morris C, Sato K, Zeng L, Viereck J, et al. Fast/Glycolytic muscle fiber growth reduces fat mass and improves metabolic parameters in obese mice. *Cell Metab* 2008;**7**:159–172.
72. Nogales-Gadea G, Pinos T, Lucia A, Arenas J, Camara Y, Brull A, et al. Knock-in mice for the R50X mutation in the PYGM gene present with McArdle disease. *Brain J Neurol* 2012;**135**:2048–2057.
73. Krag TO, Pinos T, Nielsen TL, Brull A, Andreu AL, Vissing J. Differential Muscle Involvement in Mice and Humans Affected by McArdle Disease. *J Neuropathol Exp Neurol* 2016;**75**:441–454.
74. Krag TO, Pinos T, Nielsen TL, Duran J, Garcia-Rocha M, Andreu AL, et al. Differential glucose metabolism in mice and humans affected by McArdle disease. *Am J Physiol Regul Integr Comp Physiol* 2016;**311**:R307–R314.
75. Wilcox G. Insulin and insulin resistance. *Clin Biochem Rev* 2005;**26**:19–39.
76. Guridi M, Kupr B, Romanino K, Lin S, Falchetta D, Tintignac L, et al. Alterations to mTORC1 signaling in the skeletal muscle differentially affect whole-body metabolism. *Skelet Muscle* 2016;**6**:13.
77. Argiles JM, Campos N, Lopez-Pedrosa JM, Rueda R, Rodriguez-Manas L. Skeletal Muscle Regulates Metabolism via Interorgan Crosstalk: Roles in Health and Disease. *J Am Med Dir Assoc* 2016;**17**:789–796.
78. Wolny S, McFarland R, Chinnery P, Cheetham T. Abnormal growth in mitochondrial disease. *Acta Paediatr* 2009;**98**:553–554.
79. Wolfe RR. The underappreciated role of muscle in health and disease. *Am J Clin Nutr* 2006;**84**:475–482.
80. Porter C, Hurren NM, Herndon DN, Borsheim E. Whole body and skeletal muscle protein turnover in recovery from burns. *Int J BurnsTrauma* 2013;**3**:9–17.
81. Gueugneau M, d'Hose D, Barbe C, de Barsey M, Lause P, Maiter D, et al. Increased Serpina3n release into circulation during glucocorticoid-mediated muscle atrophy. *J Cachexia Sarcopenia Muscle* 2018;<https://doi.org/10.1002/jcsm.12315>.
82. Izumiya Y, Bina HA, Ouchi N, Akasaki Y, Kharitonov A, Walsh K. FGF21 is an Akt-regulated myokine. *FEBS Lett* 2008;**582**:3805–3810.
83. Cornu M, Oppliger W, Albert V, Robitaille AM, Trapani F, Quagliata L, et al. Hepatic mTORC1 controls locomotor activity, body temperature, and lipid metabolism through FGF21. *Proc Natl Acad Sci U S A* 2014;**111**:11592–11599.
84. Minard AY, Tan SX, Yang P, Fazakerley DJ, Domanova W, Parker BL, et al. mTORC1 Is a Major Regulatory Node in the FGF21 Signaling Network in Adipocytes. *Cell Rep* 2016;**17**:29–36.

85. Khan NA, Nikkanen J, Yatsuga S, Jackson C, Wang L, Pradhan S, et al. mTORC1 Regulates Mitochondrial Integrated Stress Response and Mitochondrial Myopathy Progression. *Cell Metab* 2017;**26**:419–428, e5.
86. Luo Y, McKeethan WL. Stressed Liver and Muscle Call on Adipocytes with FGF21. *Front Endocrinol (Lausanne)* 2013;**4**:194.
87. Lin X, Liu YB, Hu H. Metabolic role of fibroblast growth factor 21 in liver, adipose and nervous system tissues. *Biomed Rep* 2017;**6**:495–502.
88. Park Y, Reyna-Neyra A, Philippe L, Thoreen CC. mTORC1 Balances Cellular Amino Acid Supply with Demand for Protein Synthesis through Post-transcriptional Control of ATF4. *Cell Rep* 2017;**19**:1083–1090.
89. Giguere V. Canonical signaling and nuclear activity of mTOR-a teamwork effort to regulate metabolism and cell growth. *FEBS J* 2018;**285**:1572–1588.
90. von Haehling S, Morley JE, Coats AJS, Anker SD. Ethical guidelines for publishing in the Journal of Cachexia, Sarcopenia and Muscle: update 2017. *J Cachexia Sarcopenia Muscle* 2017;**8**:1081–1083.